

Enhancement of coil–stretch hysteresis by self-concentration in extensional flows, and its implications for capillary thinning of liquid bridges of dilute polymer solutions

R. Prabhakar*

*Department of Mechanical & Aerospace Engineering,
Monash University, Clayton, AUSTRALIA*

(Dated: February 29, 2024)

Abstract

The coil-stretch transition in extensional flows of viscoelastic dilute polymer solutions is known to be associated with a strong hysteresis in molecular conformations and rheo-optical properties. At infinite dilution, hysteresis is caused by the large difference in frictional drag coefficient between undeformed isotropic polymer coils and highly stretched conformations. At the low extension rates in the hysteresis regime, stretched molecules pervade larger volumes than equilibrium coils since the flow is too weak to suppress transverse fluctuations. The onset of intermolecular overlap occurs for such stretched conformations at polymer concentrations much smaller than c^* , the conventional critical overlap concentration for equilibrium coils. Therefore, for a range of concentrations $c < c^*$, intramolecular hydrodynamic interactions may be significantly screened in stretched conformations. Scaling arguments based on “blob” concepts are used here to argue that the stretched state drag coefficient can grow strongly with concentration in the dilute regime. A dumbbell model with conformation-dependent drag model is used to predict a concomitant strong enhancement of coil-stretch hysteresis with increasing concentration in the dilute regime. This extensional flow induced self-concentration leads to a maximum in hysteretic effects around c^* , which progressively diminish in the semi-dilute regime where screening in isotropic coils reduces the difference in drag coefficient between stretched and coiled states. It is shown that the concentration dependence observed by Clasen *et al.* (2006) of capillary-thinning dynamics in liquid bridges of polymer solutions provides direct evidence of coil-stretch hysteresis enhancement by self-concentration.

* prabhakar.ranganathan@monash.edu

I. INTRODUCTION

Considerable theoretical insight has been achieved in recent years in understanding the dynamics of *isolated* flexible homopolymers in strong flows (Larson, 2005). It is recognized that besides chain connectivity and entropic resistance to stretching, solvent-mediated intramolecular hydrodynamic interactions play a dominant role in determining polymer dynamics even in strong flows where polymer molecules are significantly stretched. Nevertheless, our understanding of the physics at the level of *isolated* molecules has not yet translated into an ability to fully and accurately predict rheological behaviour of *dilute* polymer solutions; although much is known about their linear viscoelastic behaviour, systematic quantitative agreement of predictions from theory and simulations with experimental observations has been relatively rare well outside the equilibrium state (Larson, 2005). For instance, experiments in recent years have taken advantage of the predominantly extensional flow generated in slender filaments thinning under capillary action to probe dilute solution rheology in strongly stretching flows (McKinley and Sridhar, 2002). The mismatch between experiment and theory has been dramatically brought to the fore by Clasen *et al.* (2006) in experiments studying dynamics of capillary-thinning in liquid-bridges of dilute polymer solutions.

In such experiments, a liquid-bridge is created from a drop of a test fluid sandwiched between a pair of end-plates, by rapidly separating out the plates to a fixed distance (Anna and McKinley, 2001; Bazilevsky *et al.*, 1997, 1990; Liang and Mackley, 1994). If this distance is large enough, the bridge undergoes capillary-thinning due to the Rayleigh-Plateau instability. Polymer molecules caught in the extensional flow that develops at the necking plane undergo the coil-stretch transition. Large elastic stresses thus develop, resisting capillary action and considerably slowing down the rate at which the bridge thins.

Entov and Hinch (1997) used a stress-balance between capillary, viscous and elastic stresses to analyze inertialess capillary-thinning in a viscoelastic liquid. Using a viscoelastic model with a fixed relaxation spectrum, they showed that with exponential transient growth of the polymeric elastic stress (due to strain-hardening (SH)) becomes significantly larger than the viscous stress from the Newtonian solvent, the filament radius R decays exponentially with time t , *i.e.* $R \sim e^{-t/3\lambda_0}$, where λ_0 is the longest relaxation time; in contrast, a viscous Newtonian liquid bridge thins linearly with time. The strain-rate at the necking

plane for a slender filament is related to radial kinematics as

$$\dot{\epsilon} = -\frac{2}{R} \frac{dR}{dt}. \quad (1)$$

Further, the Weissenberg number for any extensional flow of strain-rate $\dot{\epsilon}$ is in general *defined* as

$$\text{Wi} = \dot{\epsilon} \lambda_0. \quad (2)$$

The Entov–Hinch prediction of exponential decay of filament radius thus implies that the strain-rate and Weissenberg number in the elastic regime during capillary-thinning are $\dot{\epsilon}_e = 2/(3\lambda_0)$, and $\text{Wi}_e = 2/3$, respectively.

Early experiments clearly confirmed the existence of an exponential-decay regime in capillary thinning of liquid bridges of polymer solutions (Anna and McKinley, 2001; Liang and Mackley, 1994). However, Clasen *et al.* (2006) also observed with solutions of polystyrene in high-viscosity solvents that necking in the elastic regime proceeded such that $R \sim e^{-t/3\lambda_e}$, with a relaxation-time λ_e quite different from the λ_0 characterized using small-amplitude oscillatory shear (SAOS) experiment. This implies that the observed strain-rate in the elastic regime in these experiments, $\dot{\epsilon}_e = 2/(3\lambda_e)$ corresponds to a Weissenberg number (Eqn. (2)),

$$\text{Wi}_e = \frac{2/3}{\lambda_e/\lambda_0}, \quad (3)$$

that is different from the value of $2/3$. These measurements were made across a wide range of polymer concentrations well in the dilute regime, and for several different polymer molecular weights. Similar observations have been reported on slender filaments of low-viscosity (inertia-dominant) dilute polyethylene-oxide (PEO)-in-water solutions (Tirtaatmadja *et al.*, 2006). Classical constitutive models for polymer stresses in dilute solutions such as the Oldroyd-B or FENE-P models—Entov and Hinch used a variant in their study—assume that the relaxation spectrum is solely dependent on molecular weight, but is otherwise fixed, which is contradicted by experimental observations in capillary-thinning that $\lambda_e \neq \lambda_0$. The trouble is that, once the relaxation spectrum is determined from SAOS measurements, these dilute solution models intrinsically have no mechanism that permit the relaxation time or spectrum to vary within a single sample.

An even more radical challenge to such models comes from the concentration dependence of λ_e observed in these experiments. In solutions with polymer concentrations $c \ll c^*$,

the critical overlap concentration, λ_0 is observed to depend only weakly on concentration, as expected for solutions in the dilute regime, asymptotically approaching the value λ_Z predicted by the Zimm theory for hydrodynamics of single polymers (Bird *et al.*, 1987; Doi and Edwards, 1986) in the dilute limit ($c \rightarrow 0$). In sharp contrast, λ_e increases almost linearly with c over the same range of concentrations. A dilute solution is, by definition, one where molecules are well separated from each other so that intermolecular interactions have negligible impact. The relaxation spectrum and hence λ_0 in such a solution are expected to be determined completely by average single molecule behaviour, and thus be independent of concentration. Conversely, a relaxation-time that is strongly concentration-dependent suggests the presence of strong intermolecular interactions. The observation that λ_e is concentration-dependent while λ_0 for the same samples is not, indicates that intermolecular interactions increase substantially within a single sample in the extensional flow during capillary thinning: polymer solutions “self-concentrate”!

This challenges the current modeling paradigm of classifying polymer solutions into distinct concentration regimes based on c^* determined from equilibrium size of polymeric coils, and then developing models for non-linear rheology in those regimes. Clasen *et al.* hypothesized that when polymer molecules stretch significantly, they interact hydrodynamically with each other more strongly than equilibrium coils at the same polymer concentration. This suggestion was also motivated by observations by Stoltz *et al.* (2006) of increased inter-chain interaction in multi-chain BD simulations of dilute polymer solutions in strong shear and extensional flows. The underlying reasons for the increased between stretched chains are however not yet well understood.

The key to explaining these intriguing observations may lie in another observation typical of capillary thinning (Clasen *et al.*, 2006; Tirtaatmadja *et al.*, 2006) that λ_e is considerably larger than λ_0 for a substantial range of concentrations in the dilute (in the conventional sense) regime. From Eqn. (3), this means that the observed values of Wi_e are below the Entov–Hinch prediction of $2/3$. In fact, it can be shown (as will be later, in Fig. 19 (a)) from the observed values of λ_e and λ_0 that Wi_e in these experiments are well below the critical value of $Wi_C = 1/2$ for the coil–stretch transition. These low values of Wi_e are found to be sustained for long durations (and strains). As pointed out earlier, the observed exponential decay of necking radius also means significant polymer stretching and large polymer contribution to fluid stresses at the necking plane. The combination of sustained

sub-critical Wi_e and large polymeric stresses in an extensional flow suggests a role for coil-stretch *hysteresis*.

The seminal work of De Gennes, Hinch and Tanner (De Gennes, 1974; Hinch, 1977; Tanner, 1975) showed that conformation-dependence of polymeric friction coefficient leads to hysteretic behaviour in conformational and rheo-optical properties within a window of extension rates. Steady state in extensional flow is primarily the result of a balance between internal entropic resistance of flexible polymer molecules to stretching and the frictional drag force exerted on molecules by the flowing solvent. Within the hysteresis window, nonlinearities in the dependence of the entropic resistance and drag forces on molecular stretch cause the balance between internal resistance and drag to occur at two distinct values of the stretch (Schroeder *et al.*, 2003, 2004; Sridhar *et al.*, 2007). One of these stable states corresponds to weakly deformed coils, while in the other, molecules are highly stretched. De Gennes (1974) showed that a large non-equilibrium free-energy barrier separates these two stable states for long molecules. Hysteretic behaviour thus emerges as molecules are drawn to either of these stable states depending on initial conditions (De Gennes, 1974; Hsieh and Larson, 2005; Schroeder *et al.*, 2003, 2004; Sridhar *et al.*, 2007). The coiled state becomes unstable when $Wi = Wi_C = 1/2$ and above, and molecules rapidly unravel and stretch out. The lower bound of the hysteresis window on the other hand corresponds to a critical strain rate below which the free-energy barrier vanishes and stretched molecules will always quickly relax to the coiled state. The critical Weissenberg number for this stretch-coil transition is denoted here as Wi_Σ . First predicted in the 1970s, the existence of coil-stretch hysteresis was confirmed in single-molecule experiments (Schroeder *et al.*, 2003) and BD simulations (Hsieh and Larson, 2004; Prabhakar and Prakash, 2006; Schroeder *et al.*, 2004; Sridhar *et al.*, 2007) in extensional flows.

Classical constitutive models that assume constant friction, and hence, a fixed relaxation spectrum, correctly predict a coil-stretch transition in extensional flows at $Wi_C = 1/2$, but without any hysteresis. Conformation-dependent drag thus provides for a natural mechanism for changes in relaxation times with flow, and also leads to hysteresis and the possibility of sustaining stretched states at low Wi in extensional flows, thus pointing to a possible resolution to questions posed by observations in capillary thinning. Prabhakar *et al.* (2006) therefore coupled the mid-filament stress-balance of Entov and Hinch with a multi-mode constitutive model for a dilute polymer solution that accounted for conformation-dependent

intramolecular hydrodynamic interactions in bead-spring chains. This led to an important finding: Wi_e in the elastic regime of capillary-thinning is not limited by $2/3$, but rather by the value of Wi_Σ , which is lower than $Wi_C = 1/2$.

While this provided evidence that coil–stretch hysteresis allows Wi_e to be significantly smaller than $1/2$, Prabhakar *et al.* (2006) could not predict the strong dependence of λ_e and Wi_e on concentration observed in experiments. But their dilute-solution model did not account for any *inter*-chain interactions; with any such model, the width of the hysteresis window depends solely on chain length, but is independent of concentration. Indeed, at infinite dilution, the ratio Wi_C/Wi_Σ is proportional to ratio of the mean friction coefficient of a fully-stretched rod of length L (predicted well by Batchelor’s (Batchelor, 1970) for dilute suspensions of slender rods), to ζ_Z , the (Zimm) value for isolated, isotropic coils at equilibrium. Therefore, in the dilute limit (and for solutions close to the theta state),

$$\frac{Wi_C}{Wi_\Sigma} \sim \frac{\sqrt{N_K}}{\ln N_K}, \quad (4)$$

where N_K is the number of Kuhn segments in a flexible molecule (Schroeder *et al.*, 2003, 2004; Sridhar *et al.*, 2007). With such a classical dilute-solution model with conformation-dependent drag therefore, and with $Wi_e \sim Wi_\Sigma$ in capillary thinning, Eqns. (3) and (4) above show that for any given molecular weight, the λ_e predicted mirrors the lack of significant concentration dependence of λ_0 in the dilute regime.

To this author’s best knowledge, the concentration dependence of the width of the coil–stretch hysteresis window has not been studied before. In a highly *concentrated* polymer solution, it is known that interpenetration of molecules completely screens out solvent-mediated hydrodynamic interactions (Doi and Edwards, 1986; Rubinstein and Colby, 2003). Any single molecule thus follows Rouse dynamics as opposed to Zimm hydrodynamics of isolated chains in dilute solutions. Since the Rouse friction coefficient ζ_R of a molecule is independent of conformation, hysteresis is expected to vanish in concentrated polymer solutions. If stretched molecules indeed interact more strongly than coiled molecules as suggested by Clasen *et al.* (2006), their friction coefficient could also depend more strongly on concentration. Recalling that coil–stretch hysteresis arises essentially because of differences between friction coefficients of molecules in stretched and coiled conformations, the stretched-to-coiled friction coefficient ratio could depend on concentration in solutions that are conventionally dilute under quiescent conditions. In turn, this should give rise to a

concentration-dependence in Wi_Σ at the SCT. Further, from the finding of Prabhakar *et al.* (2006) that $Wi_e = Wi_\Sigma$ in capillary-breakup, Wi_e and therefore λ_e would depend strongly on concentration, even when λ_0 does not, in the dilute regime.

Testing the hypothesis outlined above against the data of Clasen *et al.* is the primary objective of the present work. But what is the origin of the increased interaction between stretched polymers which are well separated as coils under quiescent conditions? Section II below uses insights from single-molecule BD simulations of polymer chains to propose a mechanism for self-concentration in dilute polymer solutions. Scaling arguments for hydrodynamic screening—well-established for semi-dilute solutions of coiled molecules—are then adapted for stretched chains. These results are then combined with other known scaling results to develop an interpolation scheme for the frictional drag as a function of chain stretch and concentration. This conformation-dependent friction is used then in the FENE-P dumbbell model (Bird *et al.*, 1987) for viscoelastic stress in polymer solutions. Predictions for the concentration-dependence of steady-state coil–stretch hysteresis in uniaxial extensional flow are discussed first in Section III A. The new constitutive model is used then in conjunction with a mid-filament stress balance to predict capillary thinning of nominally dilute as well semi-dilute solutions; these results are discussed in Section III B, and are compared with experimental data of Clasen *et al.* (2006). Section IV summarizes the principal conclusions of this article.

II. THE CONFORMATION-DEPENDENT DRAG MODEL

If the fluctuating end-to-end vector of a polymer molecule is $\tilde{\mathbf{Q}}$, then the average shape of a molecule in solution can be characterized by the second moment of the probability distribution for $\tilde{\mathbf{Q}}$, $\mathbf{M} = \langle \tilde{\mathbf{Q}}\tilde{\mathbf{Q}} \rangle$, the angled brackets representing an ensemble average. In the equations below, n , k_B , and T are the polymer number density, the Boltzmann constant, and the absolute solution temperature, respectively; L is the polymer contour length; $M = \text{tr} \mathbf{M} = M_{zz} + 2M_{rr} = \langle \tilde{Q}^2 \rangle$ is the mean-squared end-to-end distance in general, and the subscript ‘0’ indicates the equilibrium state of a polymer solution at a given n . In principle, the equilibrium size, and hence M_0 , are dependent on concentration, since in a good solvent, the equilibrium size is expected to decrease as concentration is increased beyond c^* and excluded-volume interactions are screened (Doi and Edwards, 1986; Rubinstein and Colby,

2003). In the model here, excluded-volume (EV) effects are ignored; EV screening is therefore not relevant in such systems, and M_0 is effectively independent of concentration. As such, predictions here are valid only for solutions close to the theta state. For chains close to the theta state, the number of Kuhn segments and the Kuhn length are defined as follows, respectively:

$$N_K = \frac{L^2}{M_0}; \quad b_K = \frac{M_0}{L}. \quad (5)$$

In the FENE-P dumbbell model (Bird *et al.*, 1987), it is customary to introduce the following two parameters in connection with the entropic resistance to molecular stretching: the “spring” constant H and the finite-extensibility (FE) parameter,

$$b = \frac{L^2 H}{k_B T}. \quad (6)$$

Here, these two parameters have been eliminated in favour of M_0 and L ; using the equilibrium prediction of the FENE-P model, we can obtain

$$H = \frac{3 k_B T}{M_0} \left(1 - \frac{M_0}{L^2} \right) = \frac{3 k_B T}{M_0} \left(1 - \frac{1}{N_K} \right), \quad (7)$$

and further,

$$b = 3 \left(\frac{L^2}{M_0} - 1 \right) = 3 (N_K - 1). \quad (8)$$

Equations for the conventional FENE-P model governing the evolution of components of \mathbf{M} can be modified to allow for a conformation-dependent friction coefficient ζ that is different from ζ_0 , the average drag coefficient at equilibrium and at a given polymer number density n (Bird and Wiest, 1985; De Gennes, 1974; Dunlap and Leal, 1987; Hinch, 1977; Phan-Thien *et al.*, 1984; Tanner, 1975). Defining the near-equilibrium relaxation time as

$$\lambda_0 = \frac{\zeta_0 M_0}{12 k_B T}, \quad (9)$$

the modified equations for the components M_{zz} and M_{rr} in a uniaxial extensional flow are:

$$\frac{dM_{zz}}{dt} = 2 \dot{\epsilon} M_{zz} - \frac{1}{\lambda_0 (\zeta/\zeta_0)} \left(f M_{zz} - \frac{M_0}{3} \right), \quad (10)$$

$$\frac{dM_{rr}}{dt} = -\dot{\epsilon} M_{rr} - \frac{1}{\lambda_0 (\zeta/\zeta_0)} \left(f M_{rr} - \frac{M_0}{3} \right), \quad (11)$$

where z represents the axial coordinate along the direction of extension, and r is the radial coordinate in the transverse direction. The ratio,

$$f(M) = \frac{L^2 - M_0}{L^2 - M}, \quad (12)$$

represents the effect of FE on stiffness of entropic resistance to stretching. At equilibrium ($\dot{\epsilon} = 0$; $t \rightarrow \infty$), $M_{zz} = M_{rr} = M_0/3$ is a solution to the equations above, and $f = 1$. In an imposed extensional flow, f diverges as $M \rightarrow L^2$, preventing M from exceeding L^2 in the model.

In polymer solutions, the flow-induced stress tensor $\boldsymbol{\tau} = -\eta_s \dot{\boldsymbol{\gamma}} + \boldsymbol{\tau}_p$, where η_s is the viscosity of the Newtonian solvent, and $\boldsymbol{\tau}_p$ is the polymer contribution to the extra stress. The only part of the stress tensor that is rheologically relevant in uniaxial extensional flows is the first normal-stress difference, $\tau_{p,zz} - \tau_{p,rr}$. The Kramers' equation for polymer stress then gives (Bird *et al.*, 1987):

$$N_{1,p} = \tau_{p,zz} - \tau_{p,rr} = -\frac{3n k_B T}{M_0} f(M_{zz} - M_{rr}); \quad (13)$$

$N_{1,p}$ vanishes at equilibrium. The polymer contribution to the extensional viscosity at any strain rate $\dot{\epsilon}$ is defined as:

$$\bar{\eta}_p = -\frac{N_{1,p}}{\dot{\epsilon}}. \quad (14)$$

The transient extensional viscosity, denoted as $\bar{\eta}_p^+$, is analogously defined when either just $N_{1,p}$, or both $N_{1,p}$ and $\dot{\epsilon}$ are time-dependent. The ODEs (10) and (11) can be integrated to steady-state to obtain predictions for steady uniaxial extensional flow at a fixed value of $\dot{\epsilon}$. For obtaining predictions for capillary-thinning of viscous liquid-bridges of polymer solutions, the ODEs above are coupled to the following stress-balance at the necking plane, obtained after neglecting the effects of fluid inertia, gravity and axial curvature of the bridge (Entov and Hinch, 1997):

$$\frac{\gamma}{R} - 3\eta_s \dot{\epsilon} + N_{1,p} = 0, \quad (15)$$

where γ is the surface tension coefficient, and the strain-rate at the mid-filament is given by Eqn. (1).

The Kramers' expression for polymer stress is strictly valid only in the dilute limit. A formal extension of the theory for solutions where intermolecular interactions are important can be expected to lead to terms explicitly of higher order in n . Instead, a mean-field

approach is taken here which models only the average behaviour of a single molecule in an effective medium consisting of the rest of the solution (Kroger, 2004). Intermolecular interactions enter the model through their influence on λ_0 and the ratio ζ/ζ_0 . For a given polymer, the coil-state friction ζ_0 and relaxation time λ_0 do not vary with the conformation and depend significantly on the polymer concentration only in the semi-dilute regime, whereas, as indicated in the Introduction, ζ is anticipated to depend both on conformation and concentration. The evolution of M_{zz} and M_{rr} is thus directly influenced by polymer concentration, which brings about a nonlinear dependence of predictions of $N_{1,p}$ on n .

Dumbbell models (De Gennes, 1974; Fuller and Leal, 1981; Hinch, 1977; Phan-Thien *et al.*, 1984; Tanner, 1975) with conformation-dependent friction are built on the observation that as chains stretch in flow, the mean friction coefficient ζ should increase monotonically from ζ_0 for equilibrium coils towards the value for fully-stretched chains. Partially stretched chains are pictured as inter-penetrable “rods” of length $\sqrt{M_{zz}}$ and diameter $\sqrt{M_{rr}}$; for notational ease, we introduce $\ell = \sqrt{M_{zz}}$ and $d = \sqrt{M_{rr}}$. Analysis of frictional properties of rods typically assume that they are slender, that is, $\ell \gg d$. Since this assumption may not always be valid for partially unravelled chains, a simple linear weighted average is used here to interpolate ζ for partially stretched chains between a value ζ_0 for equilibrium coils, and an estimate ζ_r for slender rods of length ℓ and diameter d :

$$\zeta = \frac{L - \ell}{L - d_0} \zeta_0 + \frac{\ell - d_0}{L - d_0} \zeta_r. \quad (16)$$

The sections below discuss the modeling of ζ_0 and ζ_r for various concentration regimes. The case of isolated chains is taken up first.

A. Partially stretched chains at infinite dilution

At equilibrium ($\ell = d = d_0 = \sqrt{M_0/3}$), the average friction coefficient of an isotropic coil $\zeta_0 = \zeta_Z$ at infinite dilution. For rod-like conformations, ζ_r is approximated by Batchelor’s (Batchelor, 1971) expression for slender rods:

$$\zeta_r \sim \frac{\eta_s \ell}{\ln(\ell/d)}. \quad (17)$$

The scaling result above for ζ_r cannot be used directly since the logarithmic term becomes singular when $\ell = d$. Since the Zimm friction coefficient $\zeta_Z \sim \eta_s d_0$, the following regulariza-

tion is used:

$$\zeta_r = \frac{K}{K + \ln(\ell/d)} \left(\frac{\ell}{d_0} \right) \zeta_z, \quad (18)$$

where K is an empirical constant.

Variants of the CDD model in the dilute limit such as the above are known to reproduce coil–stretch hysteresis observed in single-chain BD (De Gennes, 1974; Fuller and Leal, 1981; Hinch, 1977; Phan-Thien *et al.*, 1984; Prabhakar, 2005; Schroeder *et al.*, 2004; Tanner, 1975). Appendix A briefly discusses an approximate solution for the stretched state in steady uniaxial extensional flows. It is shown that a stretched state solution is obtained for $Wi > Wi_\Sigma$, and that $Wi_\Sigma < 1/2$ for sufficiently long chains. The constant K also controls the size of the hysteresis window in the dilute limit. Its value is chosen here to obtain a window size comparable to that observed in single-chain BD simulations; this is presented later in Fig. 3.

B. Average pervaded volume

Before proceeding further with modeling ζ for non-dilute solutions, it is necessary to examine the notions of molecular overlap and diluteness. At equilibrium, the average volume pervaded by an isotropic coil is $V_0 = d_0^3$. Therefore, for any given n , the volume fraction pervaded by polymers at equilibrium is

$$\phi_0 = n d_0^3. \quad (19)$$

The critical-overlap concentration c^* is conventionally estimated as the concentration at which coils just begin to overlap *at equilibrium*, or when $\phi_0 = 1$, which corresponds to a critical number density $n^* = 1/V_0$. This implies that the ratio $c/c^* = n/n^* = \phi_0$, and henceforth, ϕ_0 will therefore be used interchangeably with c/c^* . The average molecular pervaded volume outside equilibrium for anisotropic conformations is estimated in the conformation-tensor model as $V = \ell d^2 = \sqrt{M_{zz}} M_{rr}$. The instantaneous pervaded volume fraction is hence

$$\phi = n \ell d^2 = \phi_0 \frac{\ell d^2}{d_0^3}. \quad (20)$$

The ratio c/c^* is often used to classify polymer solutions into different concentration regimes. Equation (20) however shows that it is possible that molecular overlap may change with conformation. Upon the imposition of a flow gradient, the volume fraction ϕ will

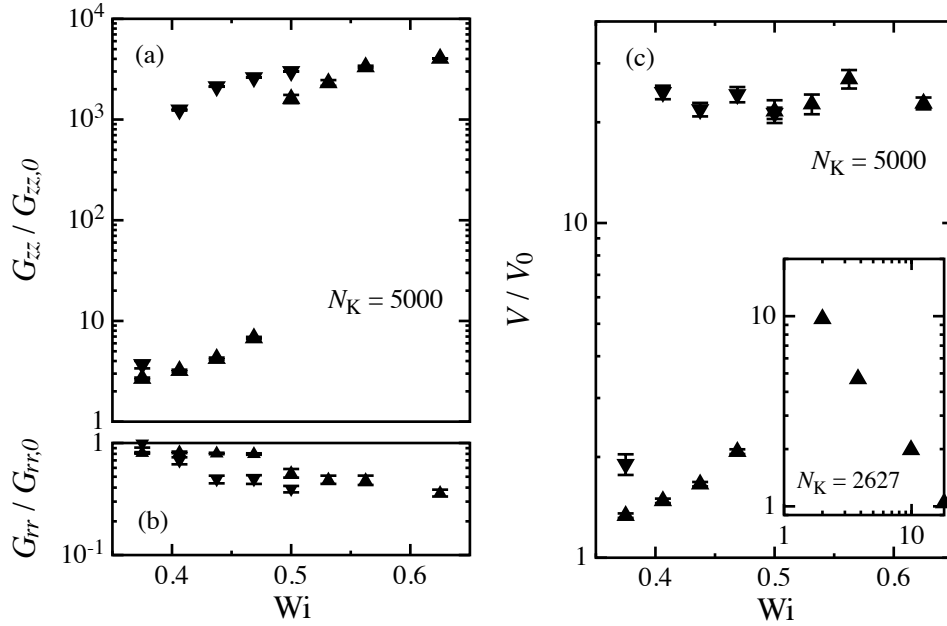


FIG. 1. Predictions of coil-stretch hysteresis in (a) gyration tensor component G_{zz} and (b) G_{rr} , and (c) pervaded volume, by BD simulations of isolated bead-spring chains: results are shown for simulations starting with initial ensembles at equilibrium (▲), and with initially stretched to 90% maximum permissible length (▼). These ensembles have different quasi-steady-states within the hysteresis window. Inset in (c) shows steady-state pervaded volume at high Wi .

remain unchanged from ϕ_0 only if molecular coils deform affinely with the incompressible solvent. Such affine deformation is only expected at high values of Wi and when FE effects are not important. But, during the elastic regime of capillary-thinning or within the coil-stretch hysteresis window, neither of these conditions may be true: as pointed out in the Introduction, $Wi \lesssim O(1)$, and chains are further significantly stretched and FE may be important.

Figure 1 shows results of BD simulations in uniaxial extensional flow obtained by starting with ensembles of either equilibrium coils or highly stretched chains, and integrating to high strains at fixed values of Wi .¹ Coil-stretch hysteresis is clearly evident in the axial and radial

¹ The molecular model for these simulations and its parameters, and the simulation algorithm have been reported in Refs. (Prabhakar and Prakash, 2004; Prabhakar *et al.*, 2004). Briefly, a polymer molecule of N_K Kuhn segments is modeled as a coarse-grained chain of beads connected by Finitely-Extensible Nonlinear Elastic (FENE) springs. Intramolecular hydrodynamic interactions are incorporated through Rotne-Prager-Yamakawa tensors. Excluded-volume interactions are neglected. Independent trajectories of chains are generated by integrating a stochastic differential equations for bead positions that describe their motion under the combined action of hydrodynamic drag forces exerted by a homogeneous flow of the surrounding solvent and its thermal fluctuations, and intramolecular connector forces.

components of the gyration tensor in Fig. 1 (a) and (b) respectively, as well as in pervaded volume, plotted in Fig. 1 (c).

It is seen that in the stretched state (upright triangles; $G_{zz} \gg G_{zz,0}$) within the hysteresis window, the values of G_{rr} are not much smaller than the equilibrium value $G_{rr,0}$. This behaviour can be understood through the approximate solution of Eqns. (10) and (11) presented in Appendix A. The transverse coil dimension in the stretched state d_s reflects the size of fluctuations in conformations transverse to the axis of the uniaxial extensional flow. In the transverse direction, Brownian fluctuations tend to relax d_s towards the equilibrium value d_0 . Opposing this, the motion of the solvent drags chain segments radially inward towards the principal axis. In addition, solvent motion along the principal axis tends to unravel and stretch a polymer chain. For stable stretched conformations, lengths are comparable to L , and FE results in increased chain stiffness, which also tends to suppress transverse excursions of a chain. From the analysis in the Appendix,

$$d_s^2 = \frac{d_0^2}{f_s + \text{Wi}(\zeta_s/\zeta_0)}. \quad (21)$$

Since entropic resistance balances axial drag, f_s is related to Wi , and

$$d_s^2 = \frac{2 \text{Wi}_\Sigma}{3 \text{Wi} \left[1 + (1 - (\text{Wi}_\Sigma/\text{Wi}))^{1/2} \right]} d_0^2. \quad (22)$$

Thus, for the stretched state, d_s is largest at the SCT where it is comparable to d_0^2 , and decreases as Wi^{-1} at higher strain-rates. This indicates that in the vicinity of the SCT neither transverse solvent drag nor nonlinear stiffness effects are strong enough to significantly dampen transverse thermal fluctuations, explaining the observations in BD simulations (Fig. 1 b).

As an aside, Eqn. (21) above is consistent with the observation that, for a chain stretched in the absence of flow by a tension applied to its ends, $d_s \sim d_0$ as long as the effects of FE are not felt and $f_s \sim 1$ (Pincus, 1976; Rubinstein and Colby, 2003). Further, Eqn. (21) shows that the transverse size predicted by the ODEs (10) and (11) is equivalent to a scaling estimate obtained by the blob argument that in strong flows transverse chain dimensions are the result of a balance between drag and transverse fluctuations (Colby *et al.*, 2007). We will return to this aspect later while calculating hydrodynamic screening lengths when stretched molecules overlap.

Large axial stretch and large transverse fluctuations in the stretched state also imply that average volumes pervaded by these conformations are much larger than at equilibrium. Indeed, from Appendix A, the stretched-state pervaded volume,

$$V_s = \sqrt{\frac{N_K}{3}} \frac{Wi_\Sigma}{Wi} V_0. \quad (23)$$

It is largest at the SCT with $V_\Sigma \sim V_0 \sqrt{N_K}$, and although it decreases as Wi^{-1} with extension-rate, at the coil-stretch transition $V_C \sim V_0 \ln N_K$ (since the ratio $Wi_C/Wi_\Sigma \sim \sqrt{N_K}/\ln N_K$). The values of N_K in the capillary-thinning experiments discussed in the Introduction are large with $\ln N_K \lesssim O(10)$ ($10^3 < N_K < 10^4$). Hence, as observed in Fig. 1 (c), stretched-state pervaded-volumes are substantially larger than those of equilibrium coils over a wide range of Wi including the hysteresis window. This also might explain observations by (Stoltz *et al.*, 2006) in multi-chain BD simulations of stronger sensitivity to chain density in rheological properties around the coil-stretch transition than at low or high Wi . They also observed more inter-chain crossings at $Wi = 1$ than at $Wi = 10$.

The analysis above suggests that the pervaded volume fraction ϕ within the hysteresis window in an extensional flow can be significantly larger than $\phi_0 = c/c^*$ at equilibrium, and thus provides a simple mechanism for self-concentration. The calculation of ζ for non-dilute solutions must therefore account for the possibility of a dynamic crossover from one concentration regime to another during extensional flow. The following sections describe how ζ is calculated given the parameters n , M_0 and L , and once the instantaneous chain dimensions ℓ and d are known.

C. Friction coefficient of equilibrium coils

The concentration dependence of ζ_0 for non-overlapping equilibrium coils due to long-range intermolecular hydrodynamic interactions is not known exactly. In dilute limit (as $c \rightarrow 0$), it is expected that the polymer contribution to the zero-shear-rate viscosity $\eta_{p,0} \sim n$, and the longest relaxation time $\lambda_0 \sim \eta_{p,0}/(n k_B T)$ is thus independent of concentration. Therefore, from Eq. (9), ζ_0 is independent of the concentration and equal to ζ_Z at low concentrations. As mentioned before, it is expected that ζ_0 will not be very different from ζ_Z when $0 < \phi_0 < 1$. When $c > c^*$, the phenomenon of hydrodynamic screening sets in. Intramolecular hydrodynamic interactions arise due to the spread of velocity perturbations in

the solvent created when any Kuhn segment moves. When chains interpenetrate, momentum in these velocity perturbations is dissipatively transferred to segments of neighbouring chains. Therefore, beyond a characteristic length-scale ξ_H (De Gennes, 1976), the presence of neighbouring chains screens out solvent velocity perturbations generated by one segment from reaching other segments of the same chain. The zone of hydrodynamic influence around each chain is thus pictured as that created by “blobs” of size ξ_H arrayed along its contour (De Gennes, 1979; Doi and Edwards, 1986; Rubinstein and Colby, 2003).

Although the existence of hydrodynamic screening is widely recognized based on observations in simulations and experiments, the underlying mechanism whereby it emerges in polymer solutions is still not fully understood (Ahlich *et al.*, 2001). A scaling estimate for the blob size ξ_H can nevertheless be derived as the average size of the neighbourhood around any segment at which the number of segments from surrounding chains just begins to exceed that of its own chain. If the number of such blobs along any chain is N_H , then the number of Kuhn segments per blob is N_K/N_H . On the other hand, in a homogeneous solution, the mean segmental density is nN_K . Hence, the argument above for ξ_H implies that

$$n N_K \xi_H^3 = \frac{N_K}{N_H},$$

or,

$$n N_H \xi_H^3 = 1. \quad (24)$$

Since $N_H \xi_H^3$ is the volume of the blobs on a single chain, the equation above means that blobs of all chains are space-filling. An additional independent equation for ξ_H and N_H comes from noting that, at equilibrium in a solution close to the theta state, chains obey ideal random-walk statistics, and

$$\xi_H^2 = b_K^2 \frac{N_K}{N_H},$$

or,

$$N_H \xi_H^2 = b_K^2 N_K = 3 d_0^2, \quad (25)$$

Ignoring pre-factors, Eqns. (25) and (24) can be solved to obtain ξ_H and N_H in terms of

ϕ_0 and d_0 (after substituting for n in terms of ϕ_0 using Eqn. (19)):

$$\xi_H = \frac{d_0}{\phi_0}; \quad N_H = \phi_0^2, \text{ when } \phi_0 \geq 1. \quad (26)$$

Since intramolecular hydrodynamic interactions persist within each blob, the Zimm-like friction coefficient of each blob ζ_H is proportional to its size, and

$$\zeta_H = \left(\frac{\xi_H}{d_0} \right) \zeta_Z = \phi_0^{-1} \zeta_Z. \quad (27)$$

Further, hydrodynamic interactions are screened between blobs, and thus each chain behaves as a Rouse chain of N_H blobs, and the overall average friction coefficient of an equilibrium coil is

$$\zeta_0 = \zeta_H N_H = \phi_0 \zeta_Z. \quad (28)$$

At critical overlap, each chain is contained within a single blob, whose friction coefficient is identical with the Zimm value for the whole chain. As ϕ_0 increases further, the screening length ξ_H decreases until it becomes comparable to a single Kuhn length, at which point screening of hydrodynamic interactions is considered to be complete. From Eqn. (26), the concentration at which $\xi_H = b_K$ and $N_H = N_K$ is

$$\phi_0^{\dagger, c} = \frac{d_0}{b_K} = \sqrt{3 N_K}. \quad (29)$$

At this concentration, a polymer coil at equilibrium is fully Rouse-like, with a maximum friction coefficient ζ_R obtained from Eqn. (28) as

$$\frac{\zeta_R}{\zeta_Z} = \phi_0^{\dagger, c} = \sqrt{3 N_K}. \quad (30)$$

For any $\phi > \phi_0^{\dagger, c}$, the friction coefficient is assumed to be constant, and equal to ζ_R .

Putting these results together along with the negligible variation ζ_0 below critical overlap,

$$\frac{\zeta_0}{\zeta_Z} = \begin{cases} 1, & \text{if } \phi_0 \leq 1, \\ \phi_0, & \text{if } 1 < \phi_0 \leq \phi_0^{\dagger, c}, \\ \sqrt{3 N_K}, & \text{if } \phi_0 > \phi_0^{\dagger, c}. \end{cases} \quad (31)$$

Next, the model for ζ_r is described for its use along with ζ_0 above in the weighted-average in Eqn. (16). As mentioned earlier, ζ_r depends not only on the instantaneous conformational components ℓ and d , but also on n through the instantaneous pervaded volume fraction ϕ . Three separate concentration regimes are identified for calculating ζ_r depending on the value of ϕ .

D. Batchelor regime for partially stretched, non-overlapping chains

Earlier, Eqn. (18) presented a regularization of Batchelor's (1970; 1971) asymptotic result for slender rods (Eqn. (17)) at infinite dilution. When $\phi_0 \neq 0$, the instantaneous volume fraction ϕ is calculated by Eqn. (20), given ϕ_0 , ℓ and d . In a non-dilute suspension of rods of length ℓ and diameter d , all aligned along the extensional axis, the mean transverse separation h between rods is such that $n\ell h^2 = 1$, and therefore from Eqn. (20),

$$\frac{h}{d} = \frac{1}{\sqrt{\phi}}. \quad (32)$$

Batchelor's result, Eqn. (17), in the dilute regime is valid when $h \gg \ell$. In that case, inter-rod interactions are negligible. Weak hydrodynamic interactions between points along each rod lead to the logarithmic term in the denominator. For non-dilute rod suspensions, when $d \ll h \ll \ell$, Batchelor (1971) showed that the only change is that the logarithmic correction has h/d as its argument: that is,

$$\zeta_r \sim \frac{\eta_s \ell}{\ln(h/d)}. \quad (33)$$

Effectively, h acts as a screening length, and points along a rod farther apart than h cannot "see" each other hydrodynamically. Batchelor (1971) suggested an interpolation between these results for dilute and non-dilute suspensions of the following form, valid for all $h \gg d$ (or $\sqrt{\phi} \ll 1$):

$$\zeta_r \sim \frac{\eta_s \ell}{\ln(\ell/d) - \ln(1 + \ell/h)}. \quad (34)$$

This expression leads to an unphysical $\zeta_r < 0$ when $\ell/d \leq 1 + \ell/h$, that is, when $\ell/d \leq (1 - \sqrt{\phi})^{-1}$. Therefore, the following regularization similar to the one in Eqn. (18) is used instead:

$$\frac{\zeta_r}{\zeta_z} = \frac{K}{K + \ln G(\ell/d, \phi)} \left(\frac{\ell}{d_0} \right), \quad (35)$$

where K is the same constant as in Eqn. (18), and the argument of the logarithmic correction in the denominator,

$$G(\ell/d, \phi) = \begin{cases} \frac{\ell/d}{1 + \ell/h} = \frac{\ell/d}{1 + (\ell/d)\sqrt{\phi}}, & \text{if } \phi < (1 - d/\ell)^2 \\ 1. & \text{if } \phi \geq (1 - d/\ell)^2 \end{cases} \quad (36)$$

This choice is consistent with Eqn. (18) when $n \rightarrow 0$, at a given ℓ and d . The equations above for ζ_r are used when $d/h = \sqrt{\phi}$ is small. The maximum value of d/h for this Batchelor regime is chosen here to be 0.1; that is, Eqns. (35) and (36) above are valid for $\phi \leq \phi_B = 0.01$. With this choice, only the first case of Eqn. (36) is required for G for all $\ell/d > 1/0.9 = 1.11$ in the Batchelor regime.

1. Transition from Batchelor regime to critical overlap

The range $\phi_B < \phi \leq 1$ then represents a transition between the Batchelor regime and the onset of critical overlap in stretched chains. To suggest an expression for ζ_r in this regime, we consider the case when $\phi = 1$ and the solution consists of closely packed anisotropic “rods” just in contact with their neighbours. For real rods, Eqn. (33) with $h = 0$ is invalid; instead, frictional drag is dominated by lubrication interactions. A polymer coil however does not have a well-defined surface where the solvent must satisfy the no-slip condition in the same sense that a rod does, and lubrication effects between coils is possibly unimportant. Instead, it is assumed that when $h \lesssim d$, screening of the weak intermolecular hydrodynamic interactions along the length of each rods (which lead to the logarithmic correction term) takes place and is complete when $h = 0$, so that when the chains just begin to overlap, each partially stretched chain behaves as a Rouse array of $N_d = \ell/d$ “beads” of size d with no hydrodynamic interactions between these beads. Intramolecular interactions are restricted within each bead whose drag coefficient is proportional to its size, that is,

$$\zeta_d = (d/d_0) \zeta_Z. \quad (37)$$

Therefore, at $\phi = 1$, the total rod-like friction coefficient is the total Rouse drag of N_d beads of friction ζ_d :

$$\frac{\zeta_r}{\zeta_Z} = N_d \frac{d}{d_0} = \frac{\ell}{d_0}. \quad (38)$$

For any ℓ and d , if the pervaded volume fraction is in the transition regime, that is, $\phi_B < \phi \leq 1$, ζ_r is calculated by linearly interpolating with respect to ϕ between the values calculated by Eqn. (43) with $\phi = \phi_B$, and by Eqn. (38) at $\phi = 1$:

$$\begin{aligned} \frac{\zeta_r}{\zeta_Z} &= \left(\frac{1 - \phi}{1 - \phi_B} \right) \left(\frac{\zeta_r}{\zeta_Z} \right)_B + \left(\frac{\phi - \phi_B}{1 - \phi_B} \right) \frac{\ell}{d_0}, \\ &= \left[\left(\frac{1 - \phi}{1 - \phi_B} \right) \left(\frac{K}{K + \ln G_B(\ell/d)} \right) + \frac{\phi - \phi_B}{1 - \phi_B} \right] \frac{\ell}{d_0} \end{aligned} \quad (39)$$

where the subscript B indicates an evaluation with Eqns. (34) and (36) for the Batchelor regime, at $\phi = \phi_B$ and with the given ℓ and d .

E. Partially stretched, overlapping chains

To my best knowledge, hydrodynamic screening within anisotropic chains when $\phi > 1$ has not been theoretically analyzed thus far. To do so, a partially stretched chain is still pictured as a linear array beads of size d as mentioned above [Fig. 2 (a)]. As in the analysis of overlapping isotropic coils, each chain is further divided into N_H blobs of size ξ_H such that the same-chain segmental density within a blob is equal to the average segmental density across the whole solution; that is, hydrodynamic blobs of all chains in the polymer solution are space-filling as before, and Eqn. (25) involving ξ_H and N_H is still valid.

Further, recalling the discussion earlier of the stretched state, the transverse size d is the length scale at which lateral thermal diffusion is balanced by the *combined* effect of chain stiffness and solvent drag; d thus represents a blob arising from the combination of nonlinear-stiffness and flow. It is reasonable to assume that within each bead of size d , lateral diffusion wins, and that the segmental distribution is equilibrium-like. Since N_k/N_H and N_k/N_d are the numbers of Kuhn segments per blob, and per bead, respectively,

$$\xi_H^2 \sim \frac{N_k}{N_H}; \quad d^2 \sim \frac{N_k}{N_d}. \quad (40)$$

The difference between the assumption above for ξ_H and the one leading to Eqn. (25) for equilibrium coils is that here the pre-factor is not assumed to be b_k^2 but the square of another local length scale arising directional persistence due to axial alignment and stretching. Indeed, using b_k^2 on the right-hand side of the equation above for d^2 suggests that ℓd is constant, which is inconsistent with the evolution equations for the conformation tensor components.

With the assumption above,

$$\frac{\xi_H^2}{d^2} = \frac{N_d}{N_H} = \frac{\ell/d}{N_H}. \quad (41)$$

Solving Eqn. (41) and (24) for ξ_H and N_H gives for partially stretched chains,

$$\xi_H = \frac{d}{\phi} = \frac{d_0^3}{\phi_0 \ell d}; \quad N_H = \phi^2 \frac{\ell}{d} = \phi_0^2 \frac{\ell^2 d}{d_0^3}, \quad \text{when } \phi \geq 1. \quad (42)$$

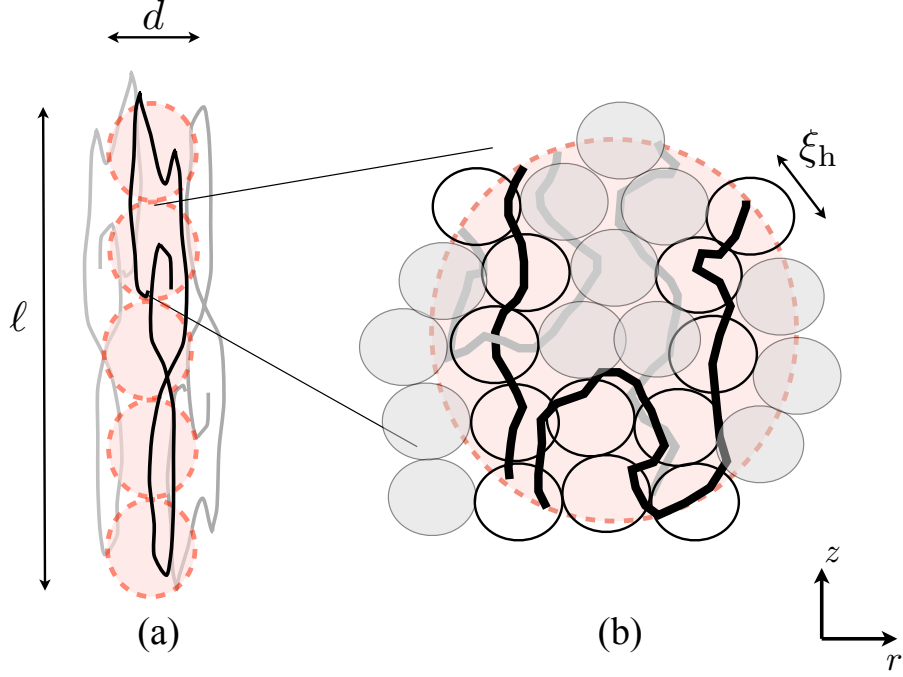


FIG. 2. Schematic of length-scales in a solution of partially unravelled, overlapping polymer chains aligned along the principal stretching direction in a uniaxial extensional flow: the black curve in (a) and (b) indicates a test chain, while the grey curves are neighbouring chains. The partially unravelled chain in (a) is pictured as a linear array of beads, each the same size as that of conformational fluctuations d transverse to the extensional axis. Within each bead, the test molecule is a chain of correlation blobs of size ξ_H . Hydrodynamic blobs from all chains are space-filling. In (b), blobs of the test chain are shown as white circles, while those of other chains are grey circles.

These are consistent with Eqns. (26) for equilibrium coils, recovering those results as $\ell \rightarrow d \rightarrow d_0$. At critical overlap, when $\phi = 1$, $\xi_H = d$: each hydrodynamic blob is the same size as a bead.

As in the case of ζ_0 for overlapping coils at equilibrium, ζ_r is calculated as the Rouse drag of N_H blobs, each with a Zimm friction $\zeta_H = (\xi_H/d_0) \zeta_Z$; hence,

$$\frac{\zeta_r}{\zeta_Z} = \frac{\xi_H}{d_0} N_H = \phi \frac{\ell}{d_0} = \phi_0 \frac{\ell^2 d^2}{d_0^4}. \quad (43)$$

For any given ℓ and d , ζ_r grows as ϕ_0 with increasing chain overlap. This is not allowed to continue indefinitely, but is limited to the maximum value of the overall free-draining Rouse

drag of a chain, given by Eqn. (30).

F. Dimensionless equations for the CDD model

For steady extensional flows at a constant $\text{Wi} = \dot{\varepsilon} \lambda_0$, there is no coupling of the conformational ODEs to an equation governing the macroscopic flow. The coupling of these equations above with the mid-filament stress balance in the case of capillary thinning is discussed later in Section III B. Rescaling the conformation tensor with M_0 as the characteristic conformation scale, and noting that $d\varepsilon = \dot{\varepsilon} dt$, the dimensionless ODEs for conformation components are:

$$\frac{dM_{zz}}{d\varepsilon} = 2 M_{zz} - \frac{1}{\text{Wi} (\zeta/\zeta_0)} \left(f M_{zz} - \frac{1}{3} \right), \quad (44)$$

$$\frac{dM_{rr}}{d\varepsilon} = -M_{rr} - \frac{1}{\text{Wi} (\zeta/\zeta_0)} \left(f M_{rr} - \frac{1}{3} \right), \quad (45)$$

where,

$$f(M) = \frac{N_K - 1}{N_K - M}. \quad (46)$$

In the absence of a macroscopic flow equation, the equilibrium relaxation time λ_0 at any given concentration ϕ_0 is chosen as the characteristic time-scale, rather than its value λ_Z at infinite dilution. With this choice, the coil-stretch transition always occurs at a fixed value of $\text{Wi} = 1/2$, whether the solution is in the dilute or semi-dilute regimes. The ODEs above for M_{zz} and M_{rr} can be integrated to steady-state. At any instant during the integration, the dimensionless ℓ and d are known from the conformation-tensor components. Hence, the instantaneous ϕ is determined using Eqn. (20). The dimensionless equivalent of the weighted-averaging in Eqn. (16) for the drag coefficient is written as:

$$\frac{\zeta}{\zeta_0} = \frac{N_K - \ell}{N_K - d_0} + \frac{\ell - d_0}{N_K - d_0} \frac{\zeta_r}{\zeta_0}, \quad (47)$$

where the dimensionless $d_0 = 1/\sqrt{3}$. The ratio ζ_r/ζ_0 is then evaluated by combining the expression for ζ_0/ζ_Z given by Eqn. (28) and those for ζ_r/ζ_Z , which are summarized in Table I). Both these ratios are limited to a maximum of ζ_R/ζ_Z . For the case of steady extensional flow, $n k_B T$ is the characteristic stress scale. Thus, the rescaled polymeric first normal-stress difference

$$N_{1,p} = \tau_{p,zz} - \tau_{p,rr} = -3 f (M_{zz} - M_{rr}). \quad (48)$$

The polymer contribution to the viscosity is rescaled by $n k_B T \lambda_0$ so that the dimensionless extensional viscosity is,

$$\bar{\eta}_p = -\frac{N_{1,p}}{\text{Wi}}. \quad (49)$$

Predictions for the standard FENE-P model are obtained by setting $\zeta/\zeta_0 = 1$ in the conformational ODEs. Thus, for steady flows, Wi and N_K are the only model parameters in the FENE-P model, whereas the CDD model additionally requires $\phi_0 = c/c^*$. The multiple steady-states for coil–stretch hysteresis are generated by fixing Wi and using $M_{zz} = M_{rr} = 1/3$ as the initial conditions for predictions for the coiled state, and $M_{zz} = 0.9N_K$ and $M_{rr} = 1/3$ as the initial conditions for the stretched state.

TABLE I. Summary of equations for the ratio ζ_r/ζ_z

ϕ	ζ_r/ζ_z
$\phi \leq \phi_B$	$\left[\frac{K}{K + \ln G} \right] \frac{\ell}{d_0}$
$\phi_B < \phi \leq 1$	$\left[\frac{K}{K + \ln G_B} \frac{1 - \phi}{1 - \phi_B} + \frac{\phi - \phi_B}{1 - \phi_B} \right] \frac{\ell}{d_0}$
$\phi > 1$	$\phi \frac{\ell}{d_0}$

III. RESULTS AND DISCUSSION

Predictions for the concentration-dependence of steady-state coil–stretch hysteresis are presented first, followed by results for capillary-thinning. These are obtained for several values of $\phi_0 = c/c^*$ in the range 10^{-4} to 100. All calculations are performed for a fixed value of $N_K = 5000$.

As the analysis in Appendix A shows, the size of the hysteresis window predicted by the CDD model depends on the constant K in Eqn. (35) for the friction coefficient in non-overlapping chains. Its value is chosen here so that the hysteresis loop predicted in the dilute limit ($\phi_0 = 0$) is comparable in size to that observed in single-chain BD simulations of flexible chains with $N_K = 5000$ (Fig. 3). A value of 0.15 gives good agreement both in the horizontal width and vertical height of the hysteresis window for the dimensionless polymer extensional viscosity, and is retained for all other calculations with the CDD model.

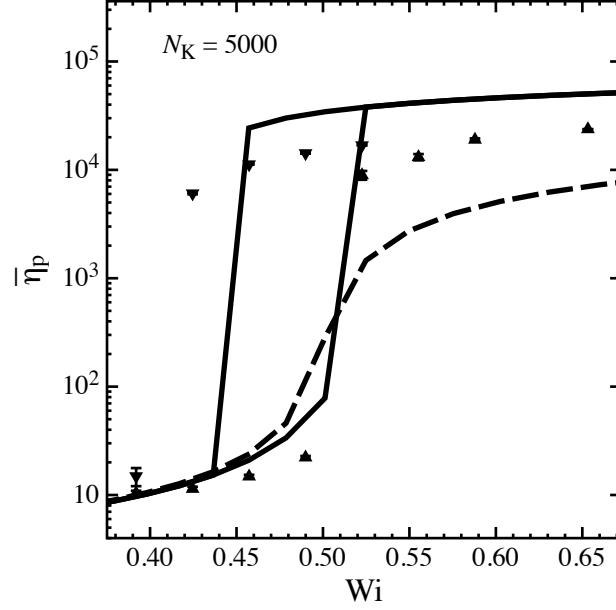


FIG. 3. Comparison of predictions of the CDD model (continuous curves) at infinite dilution for coil-stretch hysteresis in dimensionless extensional viscosity with results of single-chain BD simulations: symbols are simulation results obtained with initial ensembles consisting of equilibrium coils (▲), and of initially stretched chains (▼); the FENE-P model (dashed curve) predicts no hysteresis.

A. Self-concentration and coil-stretch hysteresis in steady uniaxial extensional flows

A strong concentration dependence is observed in the hysteresis windows predicted by the CDD model in Fig. 4. For any choice of ϕ_0 , the coil-stretch transition always occurs at $Wi_C \approx 0.5$, but Wi_Σ for the SCT transition depends on polymer concentration. As mentioned above, the choice of K ensures that the hysteresis window is similar to that observed in single-chain BD results in the limit of infinite dilution (Fig. 3; Fig. 4 (a)). With increasing concentration, Wi_Σ first *decreases* strongly with increasing concentration in the range $10^{-4} < \phi_0 < 0.1$ (Fig. 4 (a)). In the range $0.1 < \phi_0 < 1$, the width of the hysteresis window remains unchanged, but as ϕ_0 increases above 1 (Fig. 4 (b)), the hysteresis window begins to close as Wi_Σ increases and approaches $Wi_C \sim 1/2$. Hysteresis finally vanishes at large ϕ_0 values, where predictions of the CDD and conventional FENE-P models become identical. The prediction of the width of the hysteresis window as quantified by the ratio Wi_C/Wi_Σ of critical Weissenberg

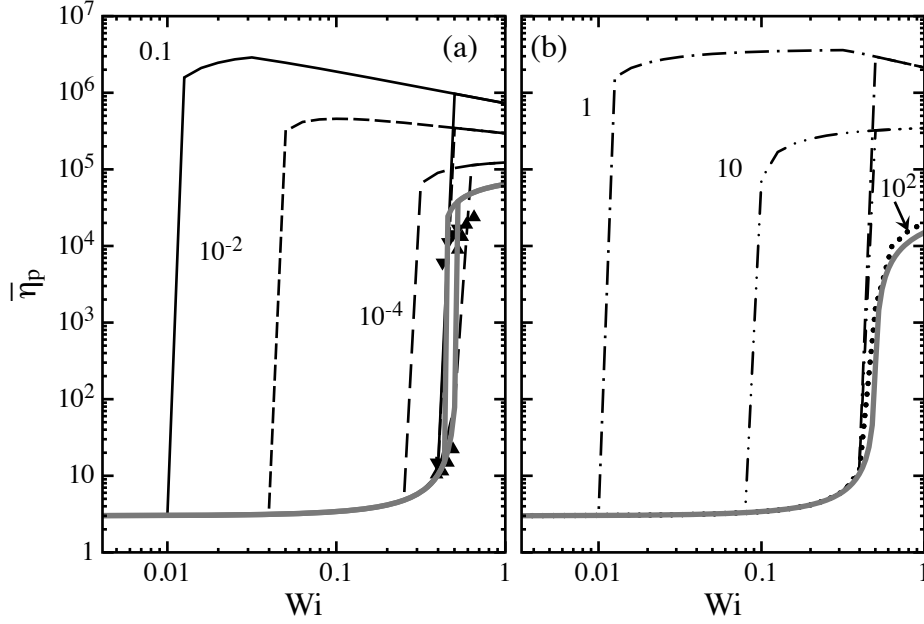


FIG. 4. Coil-stretch hysteresis in the dimensionless polymer contribution to steady-state extensional viscosity, shown for the sake of clarity separately for (a) $\phi_0 < 1$, and (b) $\phi_0 \geq 1$; numbers alongside curves indicate ϕ_0 values. Filled symbols shown in (a) are results of single-chain (*i.e.* for $\phi_0 = 0$) BD simulations. The continuous grey curves in (a) are predictions obtained with the CDD model in the infinite-dilution limit, whereas the grey curve in (b) is the hysteresis-free prediction of the FENE-P model.

numbers thus exhibits a broad maximum with respect to ϕ_0 (continuous curve in Fig. 5), the plateau at maximum spanning almost a decade in concentration for $N_K = 5000$. The maximum hysteresis window size is much larger than that at infinite dilution (horizontal line in Fig. 5).

As pointed out in the Introduction, it is known that from the analysis for dilute solutions that Wi_C/Wi_Σ is proportional to ratio of drag coefficients of stretched chains and equilibrium coils (De Gennes, 1974; Prabhakar, 2005; Schroeder *et al.*, 2004). The analysis in Appendix A shows that

$$\frac{Wi_C}{Wi_\Sigma} = \frac{\zeta_\Sigma}{\zeta_0}, \quad (50)$$

where ζ_Σ is the friction coefficient of the stable stretched state exactly at the SCT. This specific configurational state is referred to henceforth as the Σ -state. In this state, the axial and transverse chain dimensions are well approximated by (Eqn. (A12) and (A10)

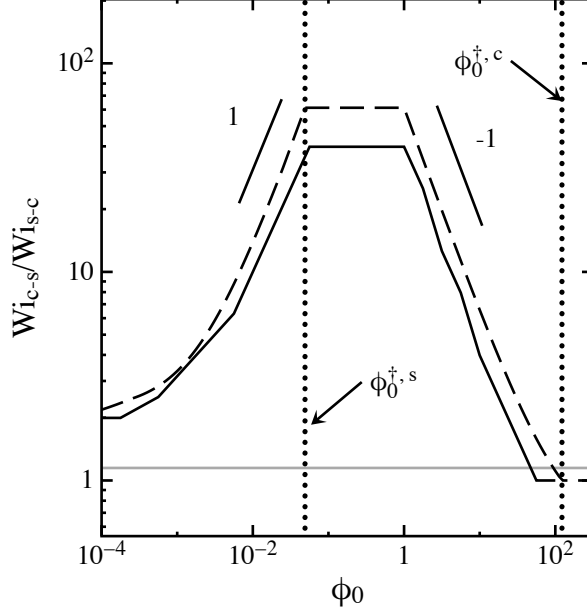


FIG. 5. Concentration-dependence of the width of the coil-stretch hysteresis window predicted by the CDD model (continuous curve): the horizontal line, $Wi_\Sigma/Wi_C \approx K\sqrt{N_K}/\ln N_K$ ($= 1.25$ for $N_K = 5000$ and $K = 0.15$), is the prediction at infinite dilution. The dashed curve is an upper bound estimated by calculating the ratio directly from the friction coefficient assuming that in the stretched state, the average axial stretch ℓ_s and transverse diameter d_s are equal to estimates derived in Appendix A for the SCT *i.e.* $\ell_\Sigma = L/2$ (Eqn. (A12)), and $d_\Sigma = \sqrt{2/3}d_0$ (Eqn. (A13)).

respectively)

$$\ell_\Sigma = \frac{L}{2}; \quad d_\Sigma = \sqrt{\frac{2}{3}}d_0. \quad (51)$$

Since chain dimensions are known for the Σ -state, it provides a handle on studying the scaling of the hysteresis-window size with respect to chain length and concentration. Figure 5 shows the estimate (dashed curve) for Wi_C/Wi_Σ directly obtained by using the chain dimensions above for calculating the friction coefficient ζ_Σ as a function of ϕ_0 ; this estimate compares well with the prediction obtained by integrating the ODEs of the CDD model to steady state (continuous curve).

The strong concentration dependence of Wi_C/Wi_Σ for values of $\phi_0 \ll 1$ and the maximum can be understood by considering the influence of the non-equilibrium pervaded volume fraction ϕ on the ratio ζ_Σ/ζ_0 . Figure 6 shows steady-state predictions by the CDD model for chain dimensions and ϕ for various equilibrium concentrations ϕ_0 . When there is significant

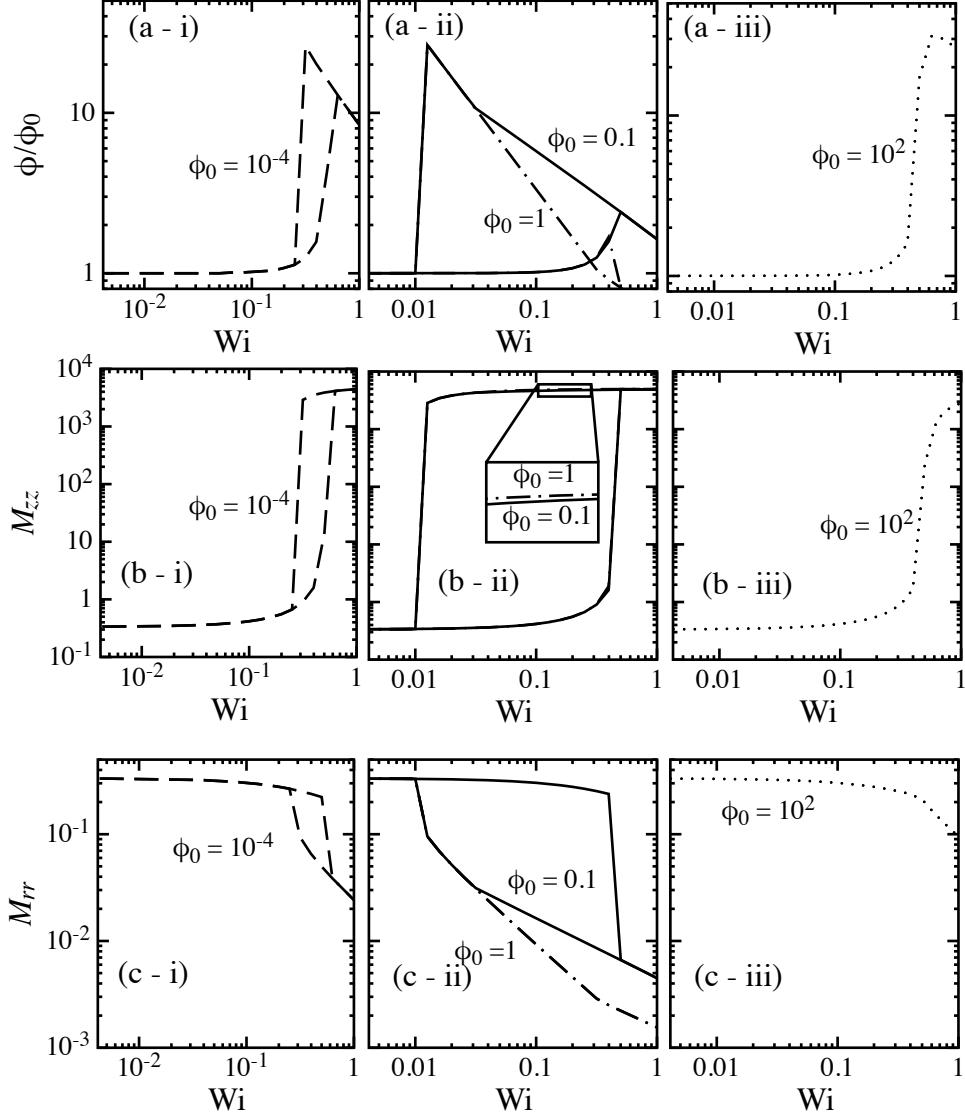


FIG. 6. Coil-stretch hysteresis in (a) pervaded volume fraction ratio ϕ/ϕ_0 , (b) M_{zz} , and (c) M_{rr} at (i) low (left column of plots), (ii) intermediate (central column), and (iii) high (right column), concentrations

hysteresis, it is clear that the largest non-equilibrium ϕ is obtained at the stretched state at the SCT. The values of the largest ϕ/ϕ_0 ratio in Fig. 6 obtained with the CDD model compare well with the approximate estimate,

$$\frac{\phi_{\Sigma}}{\phi_0} = \frac{\ell_{\Sigma}}{d_0} \left(\frac{d_{\Sigma}}{d_0} \right)^2 = \sqrt{\frac{N_K}{3}}, \quad (52)$$

derived in Appendix A. Thus, pervaded volumes at the SCT determining the friction ratio ζ_{Σ}/ζ_0 and thereby Wi_C/Wi_{Σ} can be much larger than at equilibrium.

It is useful at this stage to define critical concentrations for the Σ -state. The critical overlap concentration for overlap for equilibrium coils $\phi_0^{*,c} = 1$. Due to the larger molecular volumes in the Σ -state, overlap sets in at a lower concentration, which is obtained by setting $\phi_\Sigma = 1$ in the equation above as

$$\phi_0^{*,\Sigma} = \left(\frac{N_K}{3} \right)^{-1/2}. \quad (53)$$

Further, the critical concentration at which HI screening is complete in equilibrium coils was identified in Eqn. (29) earlier as $\phi_0^{\dagger,c} = \sqrt{3N_K}$. Its counterpart for the Σ -state is obtained by substituting in Eqn. (43) the average chain dimensions in Σ -state, and equating ζ_r/ζ_Z to $\zeta_R/\zeta_Z = \sqrt{3N_K}$:

$$\phi_0^{\dagger,\Sigma} = \frac{2\sqrt{3}}{\sqrt{N_K}}. \quad (54)$$

These four critical concentrations — $\phi_0^{*,\Sigma} < \phi_0^{\dagger,\Sigma} < \phi_0^{*,c} (= 1) < \phi_0^{\dagger,c}$ — mark key points in the concentration-dependence of Wi_C/Wi_C in Figs. 5.

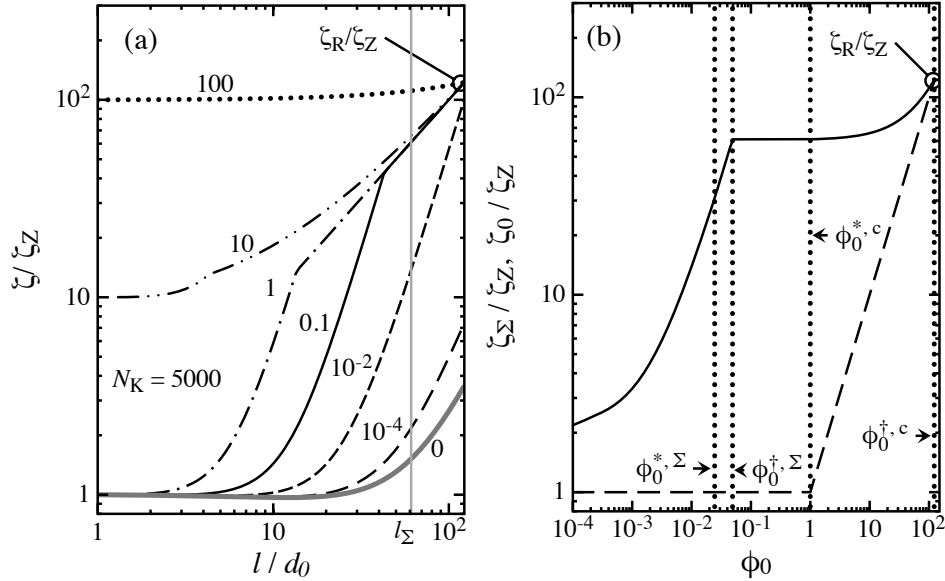


FIG. 7. The friction coefficient ratio ζ/ζ_Z at a constant transverse chain size of $d_\Sigma = \sqrt{2/3}d_0$: (a) Variation with molecular stretch ℓ for various values of ϕ_0 . The numbers alongside curves in (a) indicate ϕ_0 , while the vertical line indicates the Σ -state with $\ell_\Sigma = L/2$ (for $N_K = 5000$, $L/(2d_0) = \sqrt{3N_K}/2 = 61$). (b) Variation of ζ/ζ_Z with ϕ_0 for stretched chains at the SCT: the dashed curve in (b) shows the variation of ζ_0/ζ_Z with ϕ_0 . The maximum value for the friction coefficient ζ_R/ζ_Z and L/d_0 are both equal to $\sqrt{3N_K}$ ($= 122$ for $N_K = 5000$).

To understand changes in ζ_Σ with ϕ_0 at the stretch-coil transition, Fig. 7 (a) plots for each ϕ_0 , the average ζ/ζ_Z for a molecule as a function of its stretch with its transverse size held fixed at $d_\Sigma = \sqrt{2/3}d_0$. The grey vertical line indicates the stretch corresponding to $\ell_\Sigma = L/2$. The change in ζ_Σ/ζ_Z with ϕ_0 along this line is shown in Fig. 7 (b), along with ζ_0/ζ_Z modeled by Eqn. (31).

When $\phi_0 < 1$, the coiled-state friction remains unchanged at $\zeta_0 = \zeta_Z$. In this concentration range, when $\phi_0 \lesssim \phi_0^{*,\Sigma}$, the Σ -state friction coefficient is under transition from the Batchelor regime. When $\phi_0^{*,\Sigma} \leq \phi_0 < \phi_0^{\dagger,\Sigma}$, from Eqn. (43),

$$\frac{\zeta_\Sigma}{\zeta_Z} \approx \frac{\zeta_{r,\Sigma}}{\zeta_Z} = 2\phi_0 N_K; \quad (55)$$

that is, ζ_Σ grows linearly with concentration. Therefore, over the entire range of concentrations $\phi_0 < \phi_0^{\dagger,\Sigma}$, the ratio ζ_Σ/ζ_0 and thus the hysteresis window size Wi_C/Wi_Σ (Eqn. (50)) increases with concentration, particularly in the range $\phi_0^{*,\Sigma} \leq \phi_0 < \phi_0^{\dagger,\Sigma}$, where the increase is linear. The relative width $\phi_0^{\dagger,\Sigma}/\phi_0^{*,\Sigma} = 6$ of the concentration regime where linear concentration dependence is obtained is quite large and independent of molecular weight. In the range $\phi_0^{\dagger,\Sigma} \leq \phi_0 < 1$, neither $\zeta_\Sigma = \zeta_R$ nor ζ_0 change, and therefore ζ_Σ/ζ_0 remains constant leading to a broad plateau in the hysteresis width-versus-concentration plot, spanning a relative width of $1/\phi_0^{\dagger,\Sigma} \sim \sqrt{N_K}$.

In the nominally semidilute solution ($\phi_0 \geq 1$), the coiled-state friction coefficient $\zeta_0 = \phi_0 \zeta_Z$ while ζ_Σ remains effectively constant. (In Fig. 7 (b), a relatively small change in ζ_Σ is observed since it is calculated as a weighted-average of ζ_r and ζ_0 , according to Eqn. (16).) Therefore, when $1 \leq \phi_0 < \phi_0^{\dagger,c}$, the ratio $\zeta_\Sigma/\zeta_0 \sim \phi_0^{-1}$ and the hysteresis window shrinks correspondingly with increasing ϕ_0 , completely vanishing at $\phi_0 = \phi_0^{\dagger,c}$ when HI screening is complete in the coiled state as well. Thus, beyond $\phi_0^{\dagger,c}$, conformation-dependence of the friction coefficient disappears, and predictions are identical to those obtained with the conventional FENE-P model.

The steady-state results presented above show that self-concentration influences coil-stretch hysteresis over a broad range of concentrations spanning from about $\phi_0^{*,\Sigma}$ to $\phi_0^{\dagger,c}$, the relative size $\phi_0^{\dagger,c}/\phi_0^{*,\Sigma}$ of this concentration domain being proportional to N_K . The height of the maximum in the hysteresis width Wi_C/Wi_Σ over the asymptotic value in the dilute limit

given by Batchelor's theory is

$$\frac{(\text{Wi}_C/\text{Wi}_\Sigma)_{\text{plateau}}}{(\text{Wi}_C/\text{Wi}_\Sigma)_{\text{dil. limit}}} = \frac{\zeta_R}{\zeta_{\Sigma, \text{Batchelor}}} \approx \frac{\ln N_K}{K} \approx 10 \ln N_K. \quad (56)$$

While the dependence on molecular weight is only logarithmic, the value of the right-hand side can be large, particularly because of the factor $1/K$. Although the model presented here has ignored other numerical pre-factors, it will be shown in the following section that the estimate above provides an upper bound for the magnitude of the self-concentration effect on coil-stretch hysteresis observed in capillary-thinning experiments.

B. Capillary thinning dynamics

The results presented in the previous section are for the steady-state in steady uniaxial extensional flows. As mentioned previously, modeling capillary thinning requires coupling the ODEs for conformation tensor components with the stress-balance governing the macroscopic flow at the mid-filament plane in a liquid bridge. The mid-filament flow is further unsteady, and the strain-rate and Weissenberg number are time-dependent. The transient Weissenberg number $\text{Wi}^+ = \dot{\epsilon}(t) \lambda_0$. As before, the characteristic conformational scale is M_0 . The characteristic macroscopic length, time, and stress scales in this case are the initial mid-filament radius R_0 and $\lambda_c = 6\eta_S R_0/\gamma$ and $\tau_c = \gamma/R_0$. The pre-factor of 6 is retained in the definition of λ_c so that break-up predicted by the stress balance for the Newtonian solvent occurs at a rescaled $t = 1$.

With these choices, the dimensionless version of the stress-balance Eqn. (15) is

$$\frac{1}{R} - \frac{\dot{\epsilon}}{2} + N_{1,p} = 0. \quad (57)$$

where $\dot{\epsilon}$ above is the strain-rate rescaled by λ_c^{-1} . Ignoring an $O(1)$ universal pre-factor for solutions of long flexible molecules under theta conditions, the Zimm relaxation time,

$$\lambda_Z = \frac{\eta_S d_0^3}{k_B T} = \eta_S \frac{\phi_0}{n k_B T}. \quad (58)$$

Defining the Deborah number based on λ_Z :

$$\text{De} = \frac{\lambda_Z}{\lambda_c} = \frac{\lambda_Z}{6\eta_S R_0/\gamma}. \quad (59)$$

from Eqn. (58) above,

$$\frac{n k_B T}{\gamma/R_0} = \frac{\phi_0}{6 \text{De}}. \quad (60)$$

The polymeric first normal-stress difference from rescaled Eqn. (48) by γ/R_0 is thus

$$N_{1,p} = -\frac{\phi_0}{2 \text{De}} f(M_{zz} - M_{rr}), \quad (61)$$

where f , the FENE-P nonlinearity, is given by Eqn. (46) as before. Noting that $\lambda_0/\lambda_Z = \zeta_0/\zeta_Z$, Equation (57) can be reorganized using the definitions of Wi^+ and De to give

$$\text{Wi}^+ = \left[\frac{2 \text{De}}{R} - \phi_0 f(M_{zz} - M_{rr}) \right] \left(\frac{\zeta_0}{\zeta_Z} \right). \quad (62)$$

It is useful to note that the initial Wi^+ at $t = 0$ can be determined *a priori*, and is effectively a function De and ϕ_0 :

$$\text{Wi}^+|_{t=0} = 2 \text{De} \frac{\zeta_0}{\zeta_Z} = \begin{cases} 2 \text{De}, & \text{if } \phi_0 \leq 1, \\ 2 \text{De} \phi_0, & \text{if } 1 < \phi_0 \leq \phi_0^{\dagger,c}, \\ 2 \sqrt{3 N_K} \text{De}, & \text{if } \phi_0 > \phi_0^{\dagger,c}. \end{cases} \quad (63)$$

Treating the Hencky strain as the independent variable rather than time, the system of ODEs to solve for capillary-thinning is then

$$\frac{dt}{d\varepsilon} = \frac{1}{\dot{\varepsilon}} = \frac{\text{De}}{\text{Wi}^+}, \quad (64)$$

$$\frac{dM_{zz}}{d\varepsilon} = 2 M_{zz} - \frac{1}{\text{Wi}^+ (\zeta/\zeta_0)} \left(f M_{zz} - \frac{1}{3} \right), \quad (65)$$

$$\frac{dM_{rr}}{d\varepsilon} = -M_{rr} - \frac{1}{\text{Wi}^+ (\zeta/\zeta_0)} \left(f M_{rr} - \frac{1}{3} \right). \quad (66)$$

The instantaneous dimensionless mid-filament radius is

$$R = \exp(-\varepsilon/2). \quad (67)$$

Besides N_K and ϕ_0 , the Deborah number based on the Zimm relaxation time De appears as an additional dimensionless parameter in the capillary-thinning problem. Given these three parameters, and starting with the initial conditions $t = 0$ and $M_{zz} = M_{rr} = 1/3$ at $\varepsilon = 0$, at any $\varepsilon \geq 0$ during the forward integration, R is first determined using Eqn. (67). Since M_{zz} and M_{rr} is also known at every instant in the integration, the FENE nonlinearity

f , the instantaneous pervaded volume fraction ϕ and the friction ratios ζ/ζ_0 and ζ_0/ζ_Z are determined as previously described. The transient Weissenberg number Wi^+ is then calculated through Eqn. (62) to be substituted on the right-hand side of the ODEs above. These are integrated forward until a large terminal value of ε (typically, 20). The transient polymer contribution to the extensional viscosity is rescaled by $n k_B T \lambda_0$ as before, and hence:

$$\bar{\eta}_p = -\frac{N_{1,p}}{Wi^+}. \quad (68)$$

In order to compare this with the solvent contribution ($= 3\eta_s$), the latter is also expressed in terms of the same viscosity scale. From Eqn. (60) above and Eqn. (31) earlier for the ratio $\zeta_0/\zeta_Z = \lambda_0/\lambda_Z$,

$$\bar{\eta}_s = \frac{3\eta_s}{n k_B T \lambda_0} = \frac{3}{\phi_0 (\zeta_0/\zeta_Z)} = 3 \begin{cases} \phi_0^{-1}, & \text{if } \phi_0 \leq 1, \\ \phi_0^{-2}, & \text{if } 1 < \phi_0 \leq \phi_0^{\dagger,c}, \\ \phi_0^{-1}/\sqrt{3 N_K}, & \text{if } \phi_0 > \phi_0^{\dagger,c}. \end{cases} \quad (69)$$

Figure 8 summarizes some well-known features of predictions of the conventional FENE-P model for a typical dilute polymer solution. Initially, polymeric stresses are much smaller than the contribution from the highly viscous solvent and R is predicted to decrease linearly in time. A linear decrease in R implies an exponential increase in Wi^+ . For $De \gtrsim 1$ in a dilute solution, the initial Weissenberg number (Eqn. (63)) is further above Wi_C . This causes a rapid, nearly exponential, growth in the polymer contribution to the extensional viscosity due to SH in the initial solvent-dominated phase, and $\bar{\eta}_p$ soon outstrips the solvent contribution. The onset of the polymer-dominated phase is marked by a sudden fall in Wi^+ . In predictions for dilute solutions, the sharp decrease in Wi^+ presents as a kink in the R -vs- t curve (Fig. 8 (a)). As long as the growth in polymeric stress due to SH continues and almost completely balances the growth in capillary stress (as R^{-1}), Wi^+ remains small and may change slowly with time.

Figure 8 (d) combines the data in (b) and (c) to compare the transient $\bar{\eta}_p^+$ -vs- Wi^+ (bold curve) during capillary-thinning against the *steady-state* predictions for $\bar{\eta}_p$ (grey curve) for any value of Wi . The steady-state curve can be regarded as the infinite strain envelope limiting the capillary thinning curve, and the vertical difference between the two curves at any particular value of Wi indicates the gap that can potentially be filled by SH. As SH

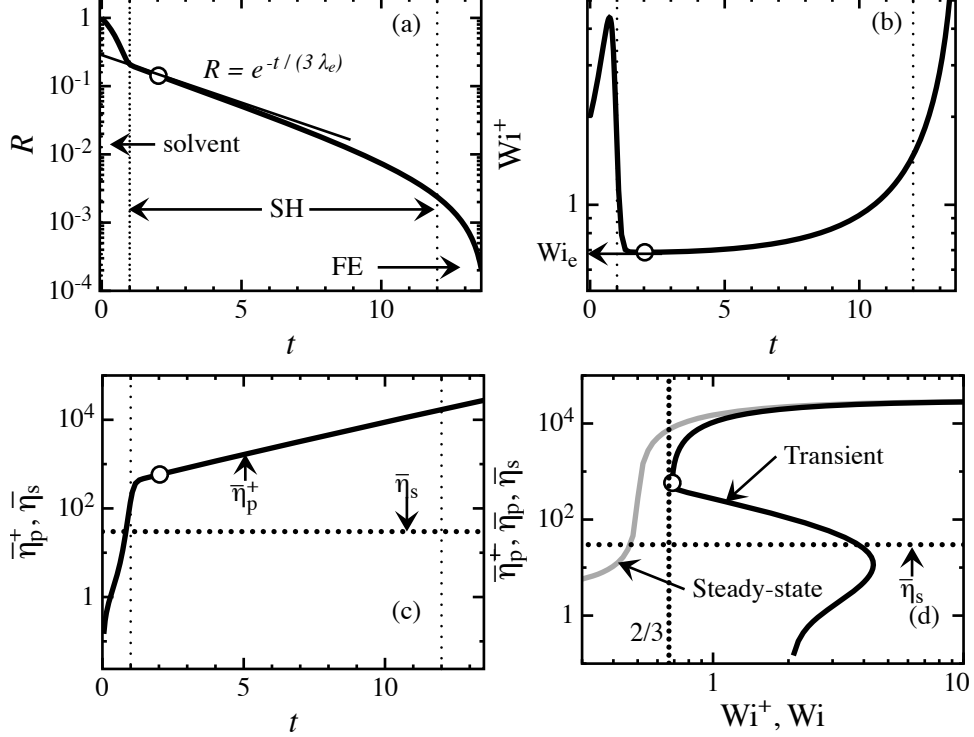


FIG. 8. Features of capillary-thinning predictions for dilute polymer solutions with the conventional FENE-P model: (a) mid-filament radius R ; (b) Weissenberg number, Wi^+ ; (c) transient (rescaled) extensional viscosities; (d) comparison of transient $\bar{\eta}_p^+$ -vs- Wi^+ with steady-state $\bar{\eta}_p$ -vs- Wi . Open symbols represent the point for determining Wi_e and λ_e . Vertical dotted lines in (a), (b) and (c) demarcate the solvent-, SH- and FE-dominated regimes, In (d), the dotted vertical line is the Entov-Hinch prediction of $Wi_e = 2/3$. In (c) and (d), the dotted horizontal line is the rescaled solvent contribution to the extensional viscosity, $\bar{\eta}_s = 3\eta_s$ (Eqn. (69)).

progresses, FE becomes important, and subsequently, it is not possible to sustain an increase in polymer viscosity by an increase in strain at fixed Weissenberg number; instead, $\bar{\eta}_p^+$ grows by tracking closely along the steady-state $\bar{\eta}_p$ -vs- Wi curve (Fig. 8 (d)). In other words, the polymer solution behaves rather as a generalized Newtonian fluid with a viscosity that depends solely on strain-rate than one that strain-hardens. Thereafter, Wi^+ must increase for flow-induced stresses to balance the capillary stress. Eventually, the polymer solution viscosity approaches a constant value, leading once more to linear decay in R and exponential growth in Wi^+ till the filament breaks up.

As Fig. 8 (b) shows, even with the conventional FENE-P model with a fairly large value of

N_k , Wi^+ is not exactly constant during the strain-hardening phase, and therefore, the decay in R is only approximately exponential. The procedure adopted here to define an effective relaxation time λ_e during this phase is equivalent to drawing a straight line with the least slope tangential to the strain-hardening portion of the R -vs- t curve on a semi-log plot. The minimum value of Wi^+ in the strain-hardening phase is first identified as Wi_e . Recalling that the Weissenberg number in this study is based on λ_0 , and since the tangential straight line is described by $R = e^{-t/(3\lambda_e)}$, the value of λ_e for a model prediction is determined as

$$\frac{\lambda_e}{\lambda_0} = \frac{2/3}{Wi_e}; \quad \frac{\lambda_e}{\lambda_Z} = \left(\frac{\lambda_0}{\lambda_Z} \right) \frac{2/3}{Wi_e}. \quad (70)$$

The results below are all for $N_k = 5000$ and $De = 1$, which are representative of the polymer solutions used by Clasen *et al.* (2006). Qualitative features of the effect of polymer concentration are discussed first by comparing predictions of the CDD and FENE-P models for five different values of ϕ_0 — 10^{-4} , 0.1, 1, 10 and 100. For reference, the critical concentrations for $N_k = 5000$ are: $\phi_0^{*,\Sigma} = 0.025$, $\phi_0^{\dagger,\Sigma} = 0.049$, $\phi_0^{*,c} = 1$, and $\phi_0^{\dagger,c} = 122$.

Figure 9 shows the transient changes in R , Wi^+ , ϕ and $\bar{\eta}_p^+$ with time t for a solution of very low concentration $\phi_0 = 10^{-4} \ll \phi_0^{*,\Sigma}$. During the solvent-dominated phase of thinning when molecules are not significantly stretched, predictions of the FENE-P and CDD models are indistinguishable from each other (at the resolution in the plots). By the time the SH phase sets in and Wi^+ falls, stretching is large enough for predictions of the two models to deviate from one another. At the low concentration in Fig. 9, the crossover to the SH phase occurs quite late since the polymer-induced stress per molecule must be large enough that its product with the low concentration is larger than the solvent contribution. As a result, both models predict an almost immediate transition to the FE dominated regime, and no distinct SH regime with a significant plateau in Wi^+ is observed in Fig. 9 (b). The brief minimum in Wi^+ is however clear, leading to kinks in the R -vs- t curves for either model. The minimum values of Wi^+ are considerably larger than $2/3$, leading to values of λ_e *much smaller than* $\lambda_0 = \lambda_Z$ (Eqn. (70)). Figure 10 shows the transient $\bar{\eta}_p^+$ -vs- Wi^+ variation relative to the steady-state results of the two models.

The instantaneous pervaded volume fraction ϕ with either model is interestingly predicted to first increase substantially in the solvent-dominated phase (Fig. 9 (c)), even though Wi^+ is quite large. As the inset in at the Fig. 9 (c) shows, although M_{rr} and hence the transverse size decrease in this phase, the growth in M_{zz} (not shown) is more than enough to compensate

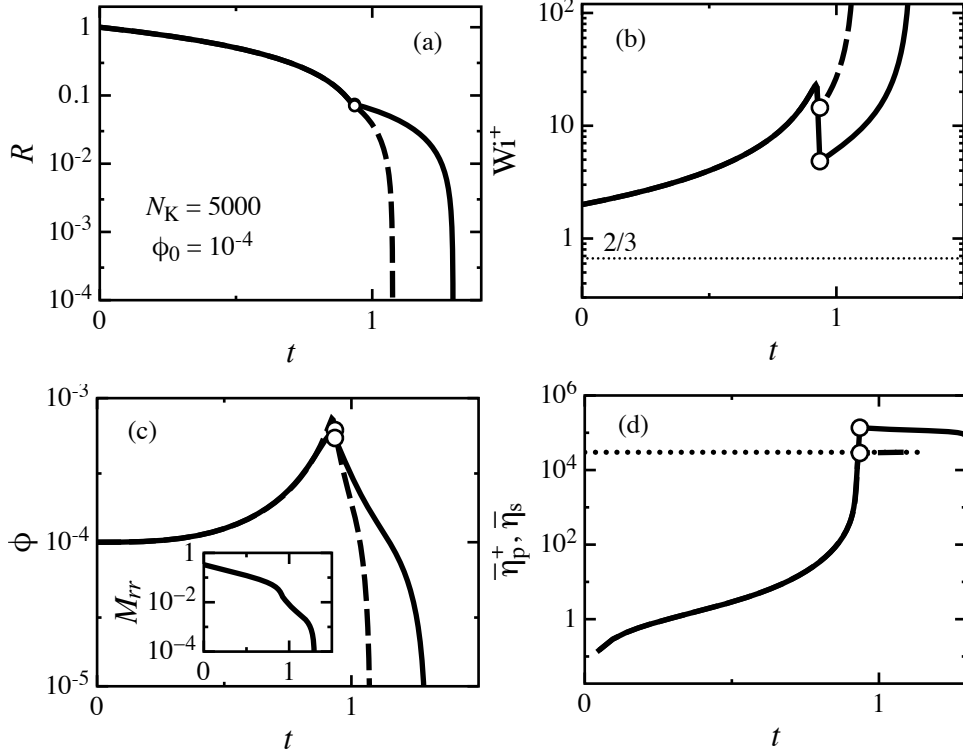


FIG. 9. Capillary-thinning dynamics at $\phi_0 = 10^{-4}$: (a) log-linear plot of mid-filament radius R versus t ; (b) transient Weissenberg number, Wi^+ ; (c) instantaneous volume fraction, ϕ ; (d) transient polymer extensional viscosity, $\bar{\eta}_p^+$. The bold continuous and dashed lines are predictions of the CDD and FENE-P models, respectively. The dotted horizontal lines in (b) and (d) represent the Entov-Hinch prediction of $Wi = 2/3$ for the elastic regime, and the dimensionless solvent viscosity (scaled by $n k_B T \lambda_0$). The inset in (c) shows the decrease of the transverse conformation tensor component M_{rr} predicted by the CDD model.

and lead to an increase in ϕ . The levelling-off of $\bar{\eta}_p^+$ in Fig. 9 (d) indicates that, in the FE dominated regime, end-to-end stretch stabilizes; the transverse size continues to shrink with increasing Wi^+ (inset in Fig. 9 (c)). As a result, chain volume fraction in the terminal regime rapidly decreases to values much lower than the equilibrium value initially.

Another notable feature of the FENE-P prediction in Fig. 9 (d) is that the FE-limited value of $\bar{\eta}_p^+$ is about the same as η_s . This implies that for much lower concentrations, the solvent contribution will be dominant even after the polymer contribution attains the FE limited plateau; in other words, the influence of the polymer will not be significant and the radial decay will be effectively identical to that of the pure solvent until break-up. As Clasen

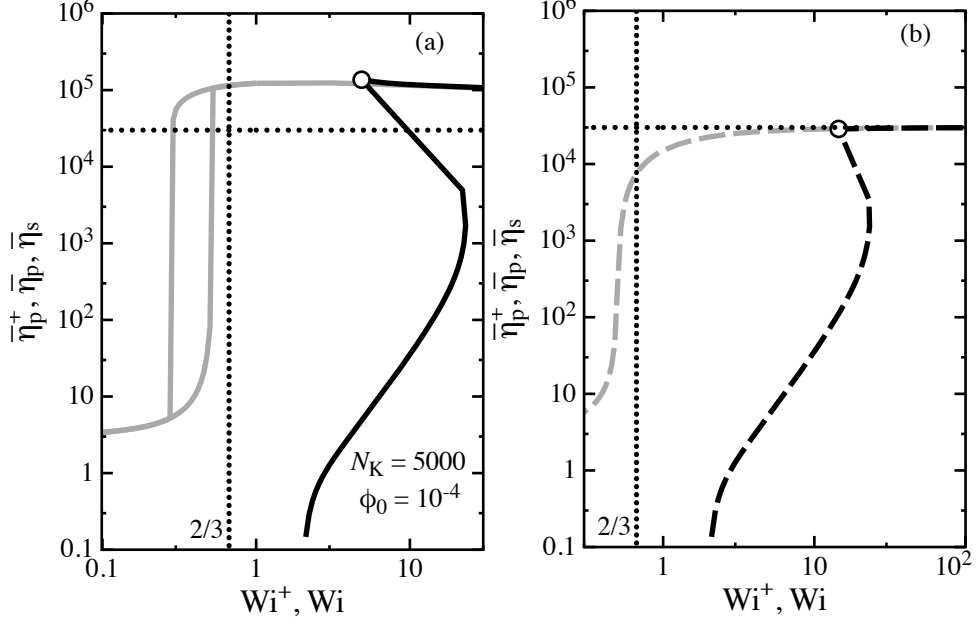


FIG. 10. Comparison of transient $\bar{\eta}_p^+$ -vs- Wi^+ variation during capillary-thinning (bold curves) with steady-state $\bar{\eta}_p$ -versus- Wi (grey curves) predictions of (a) CDD, and (b) FENE-P models, for $\phi_0 = 10^{-4}$: the dotted vertical and horizontal lines are as in Fig. 8 (d).

et al. (2006) pointed out, it is possible to calculate from the asymptotic steady-state $\bar{\eta}_p$ at full molecular stretch the value of the minimum polymer concentration required to observe a significant viscoelastic response during capillary-thinning.

Several qualitative differences emerge between the predictions of the two models progressively with increasing concentration. These are exemplified by the transient behaviour at $\phi_0 = 0.1$ in Fig. 11. The overall break-up time predicted by the CDD model becomes larger by almost two orders of magnitude. The SH phase predicted by both models is more pronounced than that observed previously at $\phi_0 = 10^{-4}$ (Fig. 11 (a) and (b)). A clear plateau of Wi^+ emerges with $Wi_e = 2/3$ in the prediction of the FENE-P model. Interestingly however, no such plateau occurs (on a logarithmic axis) with the CDD model; instead, after its sharp fall following the onset of the polymer-stress dominated SH regime, Wi^+ continues to fall *well below the value of 2/3*, attaining a very low minimum Wi_e value of about 10^{-2} . Although this corresponds to a very low value of the strain rate, the polymer viscosity $\bar{\eta}_p^+$ (Fig. 11 (d)) attained at the point of minimum Wi_e is considerably greater than the value attained by the FENE-P model for the same strain or R value of about 10^{-2} . To achieve the balance against the capillary stress corresponding to this value of R , the FENE-P model is forced to

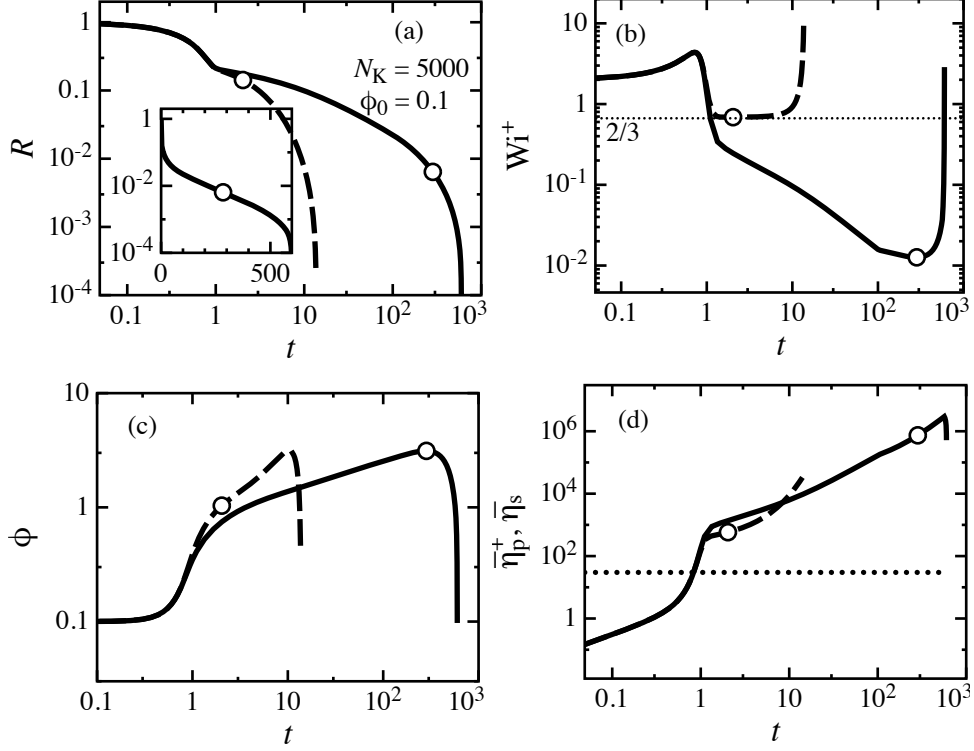


FIG. 11. Capillary-thinning dynamics at $\phi_0 = 0.1$: (a) log-log plot of mid-filament radius R versus t (inset shows log-linear plot); (b) transient Weissenberg number, Wi^+ ; (c) instantaneous volume fraction, ϕ ; (d) transient polymer extensional viscosity, $\bar{\eta}_p^+$; symbols are as in Fig. 9.

compensate for the lower value of $\bar{\eta}_p$ by attaining a higher Wi^+ . The instantaneous volume fraction (Fig. 11 (c)) in the SH regime is well beyond overlap. This self-concentration in the CDD model permits a very large extensional polymer viscosity — and therefore, a highly stretched average conformation — to be sustained at very low Wi^+ .

Figure 12 compares the transient $\bar{\eta}_p^+$ -vs- Wi^+ curves (bold curves in (a) and (b)) for the CDD and FENE-P models against their corresponding steady-state predictions (grey curves). The concentration of $\phi_0 = 0.1$ lies between the critical concentrations of $\phi_0^{\dagger, \Sigma} = 0.049$ and $\phi_0^{*, \Sigma} = 1$. Thus, the size of the steady-state hysteresis window predicted by the CDD model at this concentration is at its maximum (continuous grey curve in Fig. 12 (a)). *It is seen that the value of Wi_e attained with the CDD model is essentially the same as the stretch-coil transition Wi_{Σ} ; in sharp contrast, Wi_e with the FENE-P model is $2/3$.* The corresponding predictions of λ_e with the CDD model is therefore *considerably greater* than the value of λ_0 at the same $c/c^* = \phi_0$ (Eqn. (70)), whereas with the FENE-P model, $\lambda_e = \lambda_0$

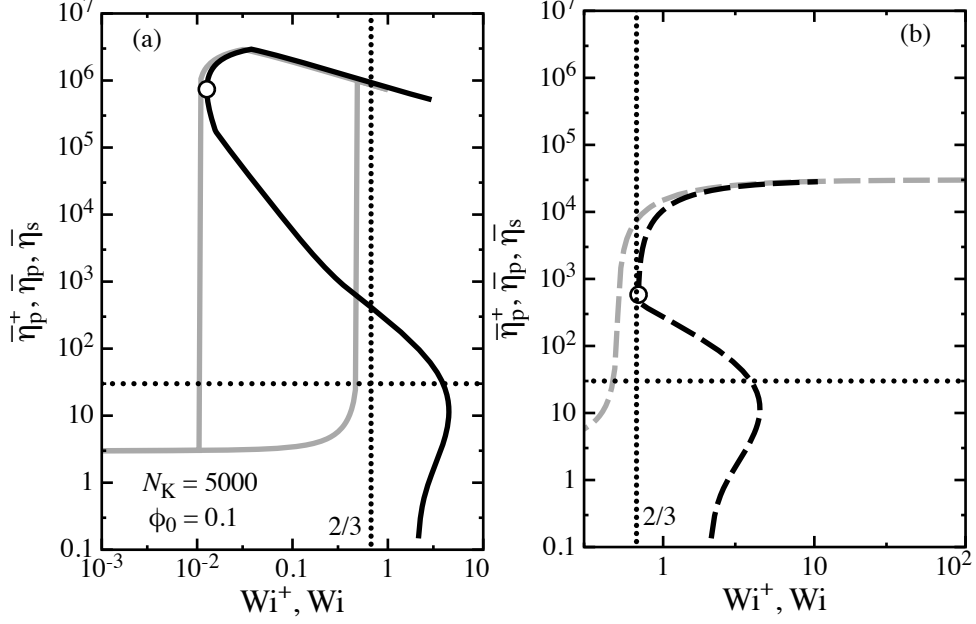


FIG. 12. Comparison of transient $\bar{\eta}_p^+$ -versus- Wi^+ variation during capillary-thinning with steady-state $\bar{\eta}_p$ -versus- Wi predictions of (a) CDD, and (b) FENE-P models, for $\phi_0 = 0.1$: symbols are as in Fig. 10.

at this concentration.

When concentration is increased further to $\phi_0 = 1$, the solution is at the edge of the semidilute domain (Fig. 13). The initial polymer contribution to the flow-induced stresses is no longer negligible in comparison with the solvent contribution. Therefore, there is no clearly distinguishable initial solvent-dominated phase. Initially, Wi^+ is nearly constant as the polymer contribution also plays an equal role in balancing the capillary stress. Since $Wi^+ > Wi_C$, rapid stretching occurs and as $\bar{\eta}_p^+$ increases Wi^+ falls. With the FENE-P, Wi^+ does not fall below $2/3$, but instead plateaus at that value. With the CDD model, on the other hand, Wi^+ continues to fall in the SH regime, again reaching a very low $Wi_e \ll 2/3$ (Fig. 13 (b)), the large $\bar{\eta}_p^+$ being the result of self-concentration (Fig. 13 (c)).

Many features of the $\bar{\eta}_p^+$ -vs- Wi_e plots in Fig. 14 for $\phi_0 = 1$ are similar to those earlier for $\phi_0 = 0.1$ in Fig. 12, particularly the fact that, as before Wi_e in the FENE-P model is bound by the Entov-Hinch limit to $2/3$ whereas, in the CDD model, $Wi_e = Wi_\Sigma$. The similarities between predictions of the CDD model for $\phi_0 = 0.1$ and 1 are due to the similarities between the steady-state hysteresis loops in $\bar{\eta}_p$ in the two cases. These two concentrations lie in the domain between $\phi_0^{\dagger, \Sigma}$ and $\phi_0^{*, c}$ in which the hysteresis window size remains unchanged

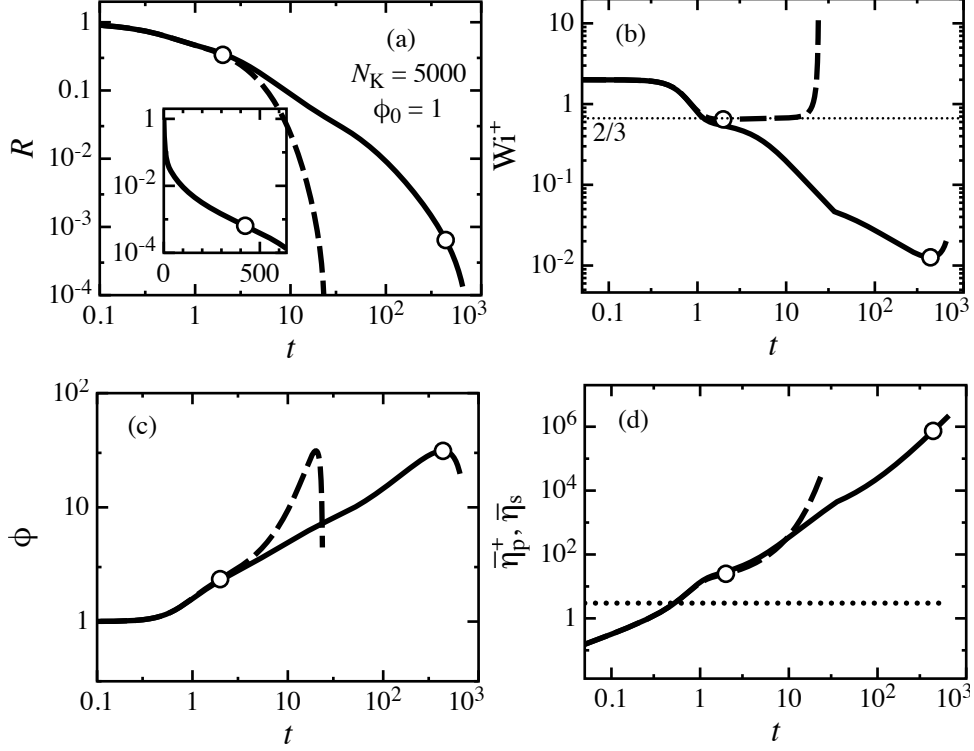


FIG. 13. Capillary-thinning dynamics at $\phi_0 = 1$: (a) log-log plot of mid-filament radius R versus t (inset shows log-linear plot); (b) transient Weissenberg number, Wi^+ ; (c) instantaneous volume fraction, ϕ ; (d) transient polymer extensional viscosity, $\bar{\eta}_p^+$; symbols are as in Fig. 9.

(Fig. 5). Thus, as at $\phi = 0.1$, $\lambda_e \gg \lambda_0 = \lambda_Z$ with the CDD model, while $\lambda_e = \lambda_0$ with the FENE-P model.

In semidilute solutions with $\phi_0 \gg 1$, the solvent contribution plays an insignificant role, even initially. As illustrated by the behaviour at $\phi_0 = 10$ in Fig. 15, the initial filament evolution is different from the rapid initial linear thinning predicted in the case of dilute solutions, with Wi^+ falling initially and increasing slowly, but remaining at low values much smaller than Wi_C . Since the polymer concentration is large, the initially low capillary stress at large $R \lesssim 1$ can be completely balanced by $\bar{\eta}_p^+$ comparable to the rescaled zero-strain-rate extensional viscosity $\bar{\eta}_{p,0} \approx 3$. Since the dominant $\bar{\eta}_p^+$ is nearly constant, the radial decay is nearly linear initially (Fig. 15 (a) inset).

In this initial phase, the transient $\bar{\eta}_p^+$ predicted by both the models tracks along the steady-state $\bar{\eta}_p$ for the *coiled* state until Wi^+ increases beyond $Wi_C = 1/2$ (Fig. 16). Thereafter, the SH regime sets in, and Wi^+ and $\bar{\eta}_p^+$ grow relatively rapidly in the FENE-P model. In this

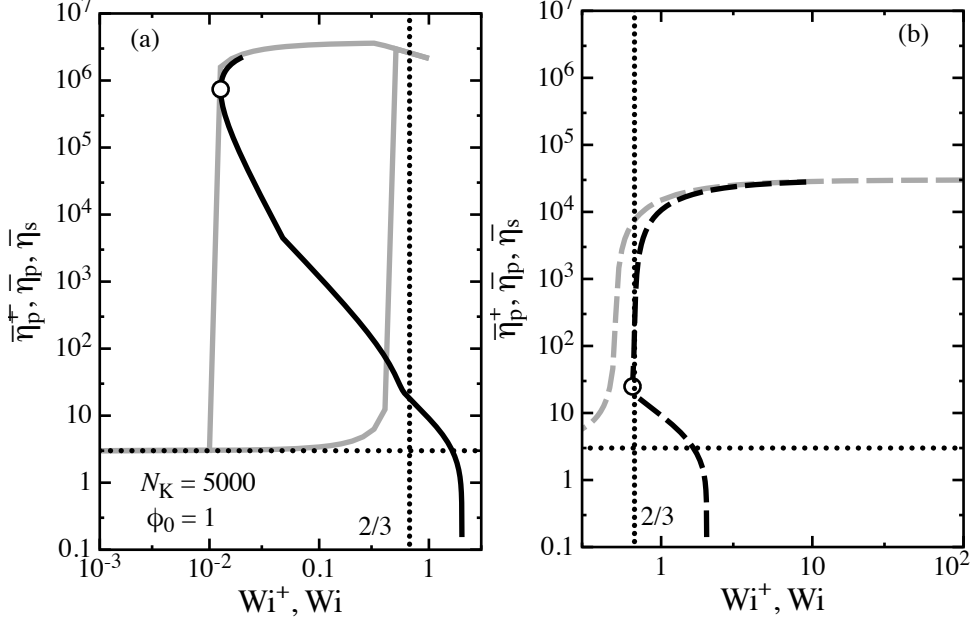


FIG. 14. Comparison of transient $\bar{\eta}_p^+$ -versus- Wi^+ variation during capillary-thinning with steady-state $\bar{\eta}_p$ -versus- Wi predictions of (a) CDD, and (b) FENE-P models, for $\phi_0 = 1$: symbols are as in Fig. 10.

case, the Entov-Hinch value is approached *from below* (Figs. 15 (b) and 16 (b)) in the FENE-P prediction, and instead of a broad minimum as observed in the previous cases, an inflection point occurs at $Wi^+ = 2/3$ (Fig. 15 (b)). Since the effective time-constant λ_e is defined in the SH regime, this inflection point is chosen as Wi_e . Thus, as before, $\lambda_e = \lambda_0$ with the FENE-P model, but since $\phi_0 > 1$, $\lambda_0 = \phi_0 \lambda_Z$ in this case. With the CDD model, the steady-state hysteresis loop causes Wi^+ to fall again after it “rounds the bend” beyond $Wi_C = 1/2$ while $\bar{\eta}_p^+$ continues to increase in the SH phase (Fig. 16 (a)). The strain-rate drops until a minimum at $Wi_e = Wi_Z$ again, before the system enters the FE limited regime, and Wi^+ grows. Since in this case $\phi_0^{*,c} < \phi_0 < \phi_0^{\dagger,c}$, the hysteresis window is significantly smaller than at $\phi_0 = 1$. The effective relaxation time $\lambda_e > \lambda_0$ again, but the ratio λ_e/λ_0 is smaller than its value at either $\phi_0 = 0.1$ or 1. Due to the smaller hysteresis window, despite the clear qualitative differences between the two models, the R -vs- t curves in Fig. 15 (a) are quite similar.

At much larger $\phi_0 \sim \phi_0^{\dagger,c}$, the friction becomes almost completely Rouse-like and independent of conformation in the CDD model. Predictions at $\phi_0 = 100$ with this model are therefore nearly identical to those of the FENE-P model. The behaviour is qualitatively

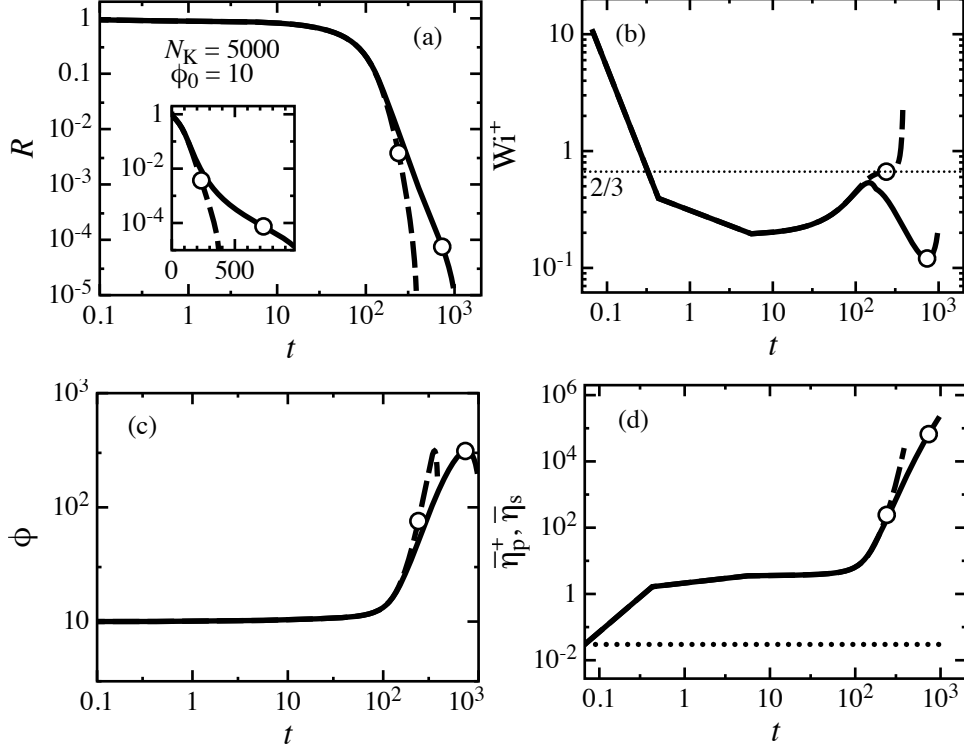


FIG. 15. Capillary-thinning dynamics at $\phi_0 = 10$: (a) log-log plot of mid-filament radius R versus t (inset shows log-linear plot); (b) transient Weissenberg number, Wi^+ ; (c) instantaneous volume fraction, ϕ ; (d) transient polymer extensional viscosity, $\bar{\eta}_p^+$; symbols are as in Fig. 9.

similar to the FENE-P prediction above for $\phi = 10$, with an inflection at $Wi_e = 2/3$ in the SH phase, but with a much more pronounced slow initial linear decay in R with the dominant polymer viscosity close to $\bar{\eta}_{p,0} \approx 3$. There is no hysteresis predicted by the CDD model at this concentration, and $\lambda_e = \lambda_0 = \phi_0 \lambda_Z$ in both models.

The results above show that beyond a certain concentration, Wi_e predicted by the CDD model in capillary-thinning is equal to the critical value Wi_Σ for the SCT. At all such concentrations λ_e/λ_0 is therefore proportional to the relative hysteresis window size, since from Eqn. (70),

$$\frac{\lambda_e}{\lambda_0} = \frac{2/3}{Wi_\Sigma} = \frac{4}{3} \frac{Wi_C}{Wi_\Sigma}. \quad (71)$$

This is seen clearly in Fig. 18 which compares the concentration-dependence of the ratio λ_e/λ_0 with that of the ratio Wi_C/Wi_Σ . Since the FENE-P model does not predict any hysteresis, λ_e/λ_0 predicted by that model levels off at 1. As mentioned in the Introduction, Prabhakar *et al.* (2006) also observed that $Wi_e = Wi_\Sigma$ with a more complex multi-mode model

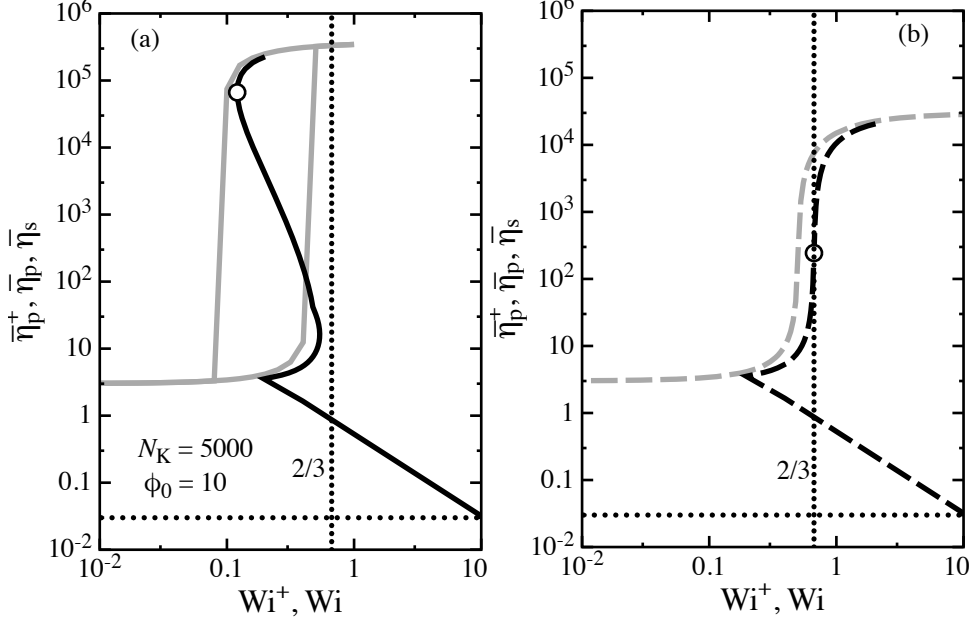


FIG. 16. Comparison of transient η_p^+ -versus- Wi^+ variation during capillary-thinning with steady-state $\bar{\eta}_p$ -versus- Wi predictions of (a) CDD, and (b) FENE-P models, for $\phi_0 = 10$: symbols are as in Fig. 10.

with conformation-dependent intramolecular HI. However, their model did not account for intermolecular interactions; the hysteresis predicted was independent of concentration and much smaller in size, comparable to that observed in single-chain BD results in Fig. 3. Their predictions for λ_e/λ_0 thus also levelled-off with concentration, but to a value larger than unity.

Model predictions are compared with the experimental data of Clasen *et al.* (2006) in Fig. 19. The experimental data shown corresponds to polystyrene samples of a range of molecular weights, in two different solvents. The equilibrium relaxation times in the experiments were obtained from SAOS measurements and are described by the empirical Martin equation, $\lambda_0/\lambda_Z = \exp(0.77 K_M \phi_0)$, where K_M is the Martin coefficient. The system-independent universal scaling relationship Eqn. (31) used for the model predictions gives a concentration dependence that is intermediate between the curves given by the Martin equations for each solvent, with $K_M = 7.5$ for polystyrene in the oligomeric-styrene Boger fluid, and 0.35 for polystyrene in DEP. The effective strain-rate values $\dot{\epsilon}_e$ were extracted by fitting straight lines tangential to the raw log R -vs- t data in the SH phase. The experimental $Wi_e = \dot{\epsilon}_e \lambda_0$ data shown in Fig. 19 (a) have been calculated using those $\dot{\epsilon}_e$ values, the λ_Z

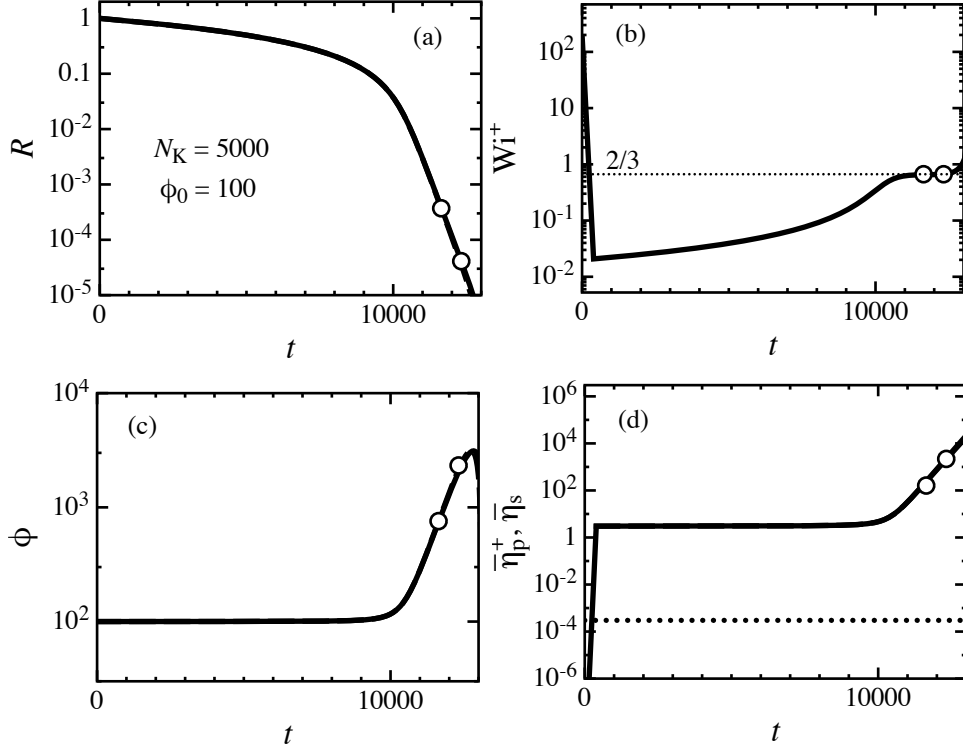


FIG. 17. Capillary-thinning dynamics at $\phi_0 = 100$: (a) log-log plot of mid-filament radius R versus t ; (b) transient Weissenberg number, Wi^+ ; (c) instantaneous volume fraction, ϕ ; (d) transient polymer extensional viscosity, $\bar{\eta}_p^+$; symbols are as in Fig. 9 (predictions of CDD and FENE-P models are identical in this case).

reported for the different samples by Clasen *et al.* and λ_0 determined at each experimental $\phi_0 = c/c^*$ using the empirical Martin equations. In other words, the experimental data are shown “as-is” from Clasen *et al.* (2006) without using any model equations developed in the present work.

The experimental Wi_e data in Fig. 19 (a) exhibit two important characteristics. Firstly, as mentioned in the Introduction, it is clear that Wi_e during the SH phase fall well below either the Entov-Hinch prediction of $2/3$ or the critical coil-stretch transition $Wi_C = 1/2$. Since these data are obtained in the regime when polymer stresses are large and dominant, the data suggest that coil-stretch hysteresis might be important in capillary-thinning dynamics. Secondly, the trend in the experimental data is in line with the observation of the minimum in Wi_e predicted by the CDD model, which results from the minimum in Wi_Σ with respect to concentration. Figure 19 (b) shows the same data in terms of the λ_e/λ_Z ratio, as presented

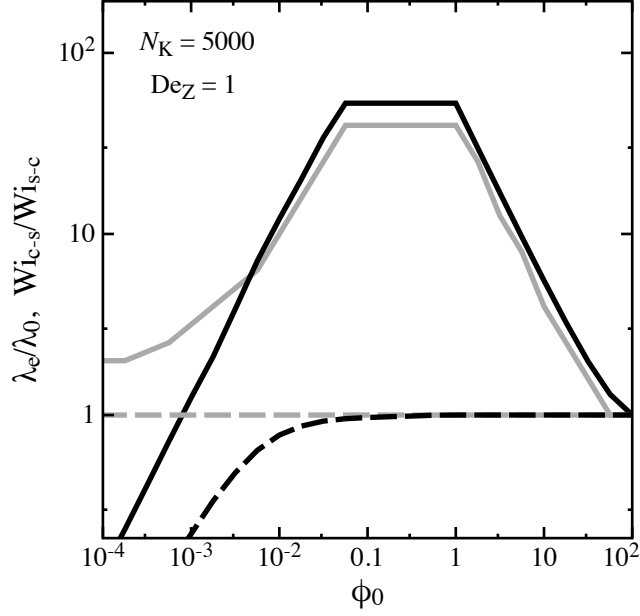


FIG. 18. Comparison of λ_e/λ_0 (bold curves) predicted during capillary-thinning with steady-state results for the size of the coil-stretch hysteresis window, Wi_C/Wi_Σ (grey curves): continuous curves - CDD model; dashed curves - FENE-P model.

Clasen *et al.*. Also shown in Fig. 19 (b) is the prediction of the conventional FENE-P model. Although the CDD model quite considerably overpredicts the experimental data, the growth in λ_e/λ_Z with concentration in the dilute regime is clearly captured by the model. It is possible that the overprediction is due to the neglect of pre-factors in the scaling results used in the model. Taken together with the FENE-P predictions, the model appears to provide bounds on the experimental data. These bounds can further be related to the polymer molecular weight in an unambiguous fashion, and can thus be of significant predictive value in practical applications.

The CDD model presented here attempts to take the physical insight contained in concepts such as blobs beyond their typical use for explaining scaling exponents and develop a phenomenological but quantitative constitutive model. Nevertheless, it is important to point out the limitations of the modeling presented here.

1. Only the slowest mode is considered; extending the model to develop a multi-mode version requires in principle considering the *dynamic* Zimm-to-Rouse crossover in the relaxation spectrum (Ahlricks *et al.*, 2001).

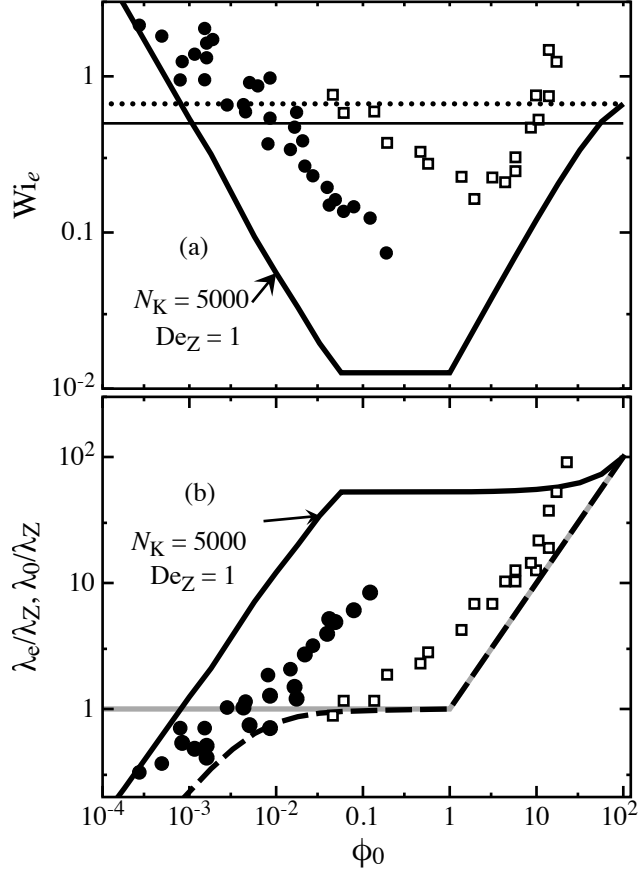


FIG. 19. Qualitative comparison of model predictions with experimental data of Clasen *et al.* (2006) for (a) Wi_e and (b) λ_e/λ_Z : filled and open symbols are data for polystyrene solutions in a mixed oligomeric styrene-dioctylphthalate solvent, and in diethylphthalate (DEP), respectively; bold continuous curves are predictions of the CDD model. Model predictions (curves) are all for a fixed value of $N_K = 5000$ and $De_Z = 1$, whereas experimental data are for a range molecular weights (corresponding to $2 \times 10^3 \lesssim N_K \lesssim 12 \times 10^3$) and Deborah numbers ($0.1 \lesssim De_Z \lesssim 1$). The continuous and dotted horizontal lines in (a) represent $Wi_C = 1/2$ for the coil–stretch transition, and the Entov–Hinch prediction of $Wi_e = 2/3$, respectively. In (b), the continuous grey curve is $\lambda_0/\lambda_Z = \zeta_0/\zeta_Z$ given by Eqn. (31), while the bold dashed line is the prediction of the FENE-P model.

2. The model neglects the influence of solvent-quality modified excluded-volume (EV) interactions and is restricted to the theta state. The experimental polystyrene systems considered by Clasen *et al.* (2006) show a significant influence of such interactions. Incorporating those effects require considering “theta blobs” and EV screening when

partially stretched chains overlap. In addition, EV interactions also influence the stiffness of the entropic resistance (Pincus, 1976), and therefore affect the coil–stretch transition and hysteresis (Radhakrishnan and Underhill, 2012; Somani *et al.*, 2010).

3. The influence of entanglements are completely ignored, which are known to become important at a concentration $\phi_0 \sim 10$; the results presented above consider ϕ_0 values well above that limit. An interesting question in this context is whether chains can become dynamically entangled due to self-concentration. Incorporating such effects into a CDD model at the dumbbell level might be possible through the “encapsulated-dumbbell” model (Bird and Deaguiar, 1983; Fang and Owens, 2005).
4. It must be pointed out here that although the values N_K and De_Z used in the modeling are comparable with the experimental values, the Ohnesorge number $Oh = \eta_S / \sqrt{\rho \gamma R_0}$ (where ρ is the solution density) varies considerably across the two solvents. This number quantifies the relative importance of viscous effects over inertio-capillary effects. The stress-balance considered in the present study neglects fluid inertia, and as such the results obtained here are valid only in the limit of $Oh \rightarrow \infty$. Among the two experimental systems of Clasen *et al.*, the polystyrene Boger fluid has $Oh \sim 10^2$ for which the inertialess stress-balance is appropriate. The polystyrene-in-DEP system on the other hand has $Oh \sim 10^{-3}$. Modeling systems of moderate or low Oh more accurately requires generalizing the stress-balance with an inertial term, as suggested by Tirtaatmadja *et al.* (2006).

The results above suggest that capillary-breakup and indeed filament-stretching extensional rheometers devices could play a vital role in discriminating between theories and models for self-concentration and thus contribute to an improved understanding of the dynamics of polymer solutions, particularly coil–stretch hysteresis. Although proposed in the 1970s, to this author’s best knowledge, there has been thus far only *one* other rheological observation of hysteresis in filament-stretching rheometry Sridhar *et al.* (2007), which together with the single-molecule studies of Schroeder *et al.* (2004), constitute the sum total of experimental evidence for this phenomenon. While the practical importance of the coil–stretch *transition* is widely appreciated, the data in Fig. 19 show that hysteresis may also play a vital role in a number of applications where capillary-thinning is relevant. The present work thus points to the need for more systematic experiments to explore the role

played by parameters such as N_K , De_z , Oh and solvent quality on capillary thinning. On the modeling front, the results here underline the necessity for detailed multi-chain BD simulations and molecular theory to develop models incorporating conformation-dependent intra- and inter-molecular HI.

It is possible that the influence of self-concentration will not be as dramatic as that observed above in all kinds of flows. The effect stems from the combination of high stretching and low strain-rates that is peculiar to the hysteretic domain in extensional flow. A similar strong effect is unlikely at steady-states in shear flow, where high stretching also requires high strain-rates, which dampen transverse fluctuations. On the other hand, self-concentration could be significant during relaxation of initially stretched chains to equilibrium after cessation of either shear or extensional flow, since transverse fluctuations and polymer stretch can be simultaneously large under those conditions.

IV. CONCLUSIONS

The principal conclusion of this work is that the anomalous concentration dependence observed in capillary-thinning experiments and multi-chain BD simulations on dilute and semidilute polymer solutions might be explained by an increased hydrodynamic interaction between chain molecules that pervaded larger volumes in flow situations that cause significant chain stretching but do not dampen transverse conformational fluctuations. Such self-concentration could lead to a strong enhancement of the phenomenon of coil-stretch hysteresis in nominally dilute polymer solutions. The enhancement is maximal over a range of concentrations well below the $c/c^* = 1$, and progressively diminishes in the semidilute regime.

ACKNOWLEDGMENTS

This work was supported by a CPU-time grant on the National Computational Infrastructure at the Australian National University, Canberra, and a monetary grant from the Australian Research Council (Discovery Project No. DP120101322). The author is indebted to Ravi Jagadeeshan, Burkhard Duenweg, Gareth McKinley, Tam Sridhar and David Boger for their insight, advice and encouragement.

Appendix A: Analysis of the stable stretched state in steady uniaxial extensional flow

The qualitative features of coil–stretch hysteresis in the dilute limit have been in the past explained by considering the the steady-state probability distribution of end-to-end stretch in uniaxial extensional flow of a dumbbell with conformation-dependent friction (De Gennes, 1974; Schroeder *et al.*, 2003, 2004). The CDD model presented in the current work also captures many of the important features.

At steady state for a give extension rate $\dot{\epsilon}$,

$$0 = 2 \dot{\epsilon} \ell^2 - \frac{1}{\lambda_0 (\zeta/\zeta_0)} (f \ell^2 - d_0^2), \quad (\text{A1})$$

$$0 = -\dot{\epsilon} d^2 - \frac{1}{\lambda_0 (\zeta/\zeta_0)} (f d^2 - d_0^2). \quad (\text{A2})$$

From the exact results, one expects that in the stable stretched state (denoted by the subscript ‘s’), $f_s \ell_s^2 \gg d_0^2 \gtrsim d^2$. Substituting this approximation in Eqn. (A2) above,

$$f_s = 2 \text{Wi} \frac{\zeta_s}{\zeta_0}. \quad (\text{A3})$$

Assuming that $\zeta_s \approx \zeta_r$ in the stretched state, from the equations for ζ_r/ζ_Z in Table I and Eqn. (31), ζ_s/ζ_0 is of the form $\zeta_s/\zeta_0 = C \ell_s/d_0$. In general, C is itself a function of the conformation, but in situations when C is nearly constant, an approximate solution can be obtained. This occurs in the dilute limit, and when HI screening is close to complete in the stretched state and $\zeta_r \approx \zeta_R$. Formally, a detailed analysis of the stretched state requires a perturbation expansion of all terms depending on ℓ_s as $\ell_s = L(1 - \epsilon + \dots)$. For the sake of clarity, C is assumed to be constant below, which yields qualitatively similar results although with different pre-factors.

$$f_s = 2 C \text{Wi} \frac{\ell_s}{d_0}. \quad (\text{A4})$$

From the definition of f in Eqn (12), in the stretched state

$$f_s \approx \frac{L^2}{L^2 - \ell_s^2} \approx \frac{L}{2(L - \ell_s)}. \quad (\text{A5})$$

Equating the two expressions above for f_s gives a quadratic equation for ℓ_s/L :

$$\frac{\ell_s}{L} \left(1 - \frac{\ell_s}{L}\right) - \frac{d_0}{4 \text{Wi} C L} = 0, \quad (\text{A6})$$

which has real roots when Wi is greater than the critical value

$$Wi_{\Sigma} = \frac{d_0}{C L} = \frac{1}{C \sqrt{3 N_K}}, \quad (A7)$$

since $L/d_0 = \sqrt{3 N_K}$.

Thus, the constant C can be eliminated in favour of Wi_{Σ} . For $Wi > Wi_{\Sigma}$, ℓ_s for the stable stretched state corresponds is given by the root of the quadratic equation above:

$$\ell_s = \frac{L}{2} \left[1 + \left(1 - \frac{Wi_{\Sigma}}{Wi} \right)^{1/2} \right], \quad (A8)$$

and ℓ_s approaches L with increasing Wi . Substituting for C and ℓ_s in Eqn. (A4),

$$f_s = \frac{Wi}{Wi_{\Sigma}} \left[1 + \left(1 - \frac{Wi_{\Sigma}}{Wi} \right)^{1/2} \right]. \quad (A9)$$

Considering next Eqn. (A2) for the transverse size d_s in the stretched state,

$$\left(\frac{d_s}{d_0} \right)^2 = \frac{1}{f_s + Wi (\zeta_s/\zeta_0)} = \frac{1}{3 Wi (\zeta_s/\zeta_0)} = \frac{2}{3 f_s} = \frac{2 Wi_{\Sigma}}{3 Wi \left[1 + \left(1 - (Wi_{\Sigma}/Wi) \right)^{1/2} \right]}. \quad (A10)$$

The pervaded volume $V = \ell d^2$; in the stretched state therefore, from Eqns. (A8) and (A10) above,

$$\frac{\phi_s}{\phi_0} = \frac{V_s}{V_0} = \left(\frac{\ell_s}{d_0} \right) \left(\frac{d_s}{d_0} \right)^2 = \frac{1}{3} \frac{L/d_0}{Wi/Wi_{\Sigma}} = \frac{\sqrt{N_K/3}}{Wi/Wi_{\Sigma}}. \quad (A11)$$

Therefore, transverse chain dimensions and volume are largest at the SCT and decrease with increasing strain-rate effectively as Wi^{-1} .

Chain dimensions at the stable stretched state just at the SCT are obtained by setting $Wi = Wi_{\Sigma}$ in the relations above. This state is referred to as the Σ -state, and values therein are denoted with the subscript Σ . Thus, from Eqn. (A8),

$$\frac{\ell_{\Sigma}}{d_0} = \frac{L}{2 d_0} = \frac{\sqrt{3 N_K}}{2}, \quad (A12)$$

$$\left(\frac{d_{\Sigma}}{d_0} \right)^2 = \frac{2}{3}, \quad (A13)$$

$$\frac{V_{\Sigma}}{V_0} = \frac{\phi_{\Sigma}}{\phi_0} = \sqrt{\frac{N_K}{3}}. \quad (A14)$$

Further, from Eqn. (A9), $f_{\Sigma} = 1$ in the Σ -state; therefore, from Eqn. (A3),

$$2 Wi_{\Sigma} \frac{\zeta_{\Sigma}}{\zeta_0} = 1,$$

or equivalently,

$$\dot{\epsilon}_{\Sigma} \left(\lambda_0 \frac{\zeta_{\Sigma}}{\zeta_0} \right) = \dot{\epsilon}_{\Sigma} \lambda_{\Sigma} = \frac{1}{2}. \quad (\text{A15})$$

The equation above shows that the SCT occurs when a Weissenberg number defined with a polymer relaxation-time characteristic of the stretched state— $\lambda_{\Sigma} = \lambda_0(\zeta_{\Sigma}/\zeta_0)$ —attains a value of 1/2. Noting that $\text{Wi}_C = 1/2$, the width of the hysteresis window is obtained as

$$\frac{\text{Wi}_C}{\text{Wi}_{\Sigma}} = \frac{\zeta_{\Sigma}}{\zeta_0}. \quad (\text{A16})$$

-
- Ahlrichs, P., R. Everaers and B. Dünweg, “Screening of hydrodynamic interactions in semidilute polymer solutions: A computer simulation study,” *Phys. Rev. E* **64**, 040501 (2001).
- Anna, S. L. and G. H. McKinley, “Elasto-capillary thinning and breakup of model elastic liquids,” *J. Rheol.* **45**, 115–138 (2001).
- Batchelor, G. K., “Slender-body theory for particles of arbitrary cross-section in Stokes flow,” *J. Fluid. Mech.* **44**, 419–440 (1970).
- Batchelor, G. K., “Stress generated in a non-dilute suspension of elongated particles by pure straining motion,” *J. Fluid Mech.* **46**, 813–829 (1971).
- Bazilevsky, A. V., V. M. Entov, M. M. Lerner and A. N. Rozhkov, “Failure of polymer solution filaments,” *Polym. Sci. Ser. A Ser. B* **39**, 316–324 (1997).
- Bazilevsky, A. V., V. M. Entov and A. N. Rozhkov, “Liquid filament microrheometer and some of its applications,” in *Proc. Third Euro. Rheol. Conf.*, ed. D. R. Oliver, pp. 41–43 (1990).
- Bird, R. B., C. F. Curtiss, R. C. Armstrong and O. Hassager, *Dynamics of Polymeric Liquids*, vol. 2. Kinetic theory, Wiley-Interscience, New York, 2 edn. (1987).
- Bird, R. B. and J. Deaguiar, “An encapsulated dumbbell model for concentrated polymer solutions and melts I. Theoretical developments and constitutive equation.” *J. Non-Newtonian Fluid Mech.* **13**, 149–160 (1983).
- Bird, R. B. and J. M. Wiest, “Anisotropic effects in dumbbell kinetic-theory,” *J. Rheol.* **29**, 519–532 (1985).
- Clasen, C., J. P. Plog, W. M. Kulicke, M. Owens, C. Macosko, L. Scriven, M. Verani and G. McKinley, “How dilute are dilute solutions in extensional flows?” *J. Rheol.* **50**, 849–881 (2006).

- Colby, R. H., D. C. Boris, W. Krause and S. Dou, “Shear thinning of unentangled flexible polymer liquids,” *Rheologica Acta* **46**, 569–575 (2007).
- De Gennes, P., “Coil-stretch transition of dilute flexible polymers under ultrahigh velocity-gradients,” *J. Chem. Phys.* **60**, 5030–5042 (1974).
- De Gennes, P., “Dynamics of entangled polymer solutions. II. Inclusion of hydrodynamic interactions,” *Macromolecules* **9**, 594–598 (1976).
- De Gennes, P.-G., *Scaling concepts in polymer physics*, Cornell University Press (1979).
- Doi, M. and S. F. Edwards, *The Theory of Polymer Dynamics*, Oxford University Press (1986).
- Dunlap, P. N. and L. G. Leal, “Dilute polystyrene solutions in extensional flows: birefringence and flow modification,” *J. Non-Newtonian Fluid Mech.* **23**, 5–48 (1987).
- Entov, V. M. and E. J. Hinch, “Effect of a spectrum of relaxation times on the capillary thinning of a filament of elastic liquid,” *J. Non-Newtonian Fluid Mech.* **72**, 31–53 (1997).
- Fang, J. and R. G. Owens, “New constitutive equations derived from a kinetic model for melts and concentrated solutions of linear polymers,” *Rheol. Acta* **44**, 577–590 (2005).
- Fuller, G. G. and L. G. Leal, “The effects of conformation-dependent friction and internal viscosity on the dynamics of the nonlinear dumbbell model for a dilute polymer solution,” *J. Non-Newtonian Fluid Mech.* **8**, 271–310 (1981).
- Hinch, E. J., “Mechanical models of dilute polymer-solutions in strong flows,” *Phys. Fluids* **20**, S22–S30 (1977).
- Hsieh, C.-C. and R. G. Larson, “Modeling hydrodynamic interaction in brownian dynamics: Simulations of extensional and shear flows of dilute solutions of high molecular weight polystyrene,” *J. Rheol.* **48**, 995–1021 (2004).
- Hsieh, C.-C. and R. G. Larson, “Prediction of coil-stretch hysteresis for dilute polystyrene molecules in extensional flow,” *J. Rheol.* **49**, 1081–1089 (2005).
- Kroger, M., “Simple models for complex nonequilibrium fluids,” *Phys. Rep.* **390**, 453–551 (2004).
- Larson, R. G., “The rheology of dilute solutions of flexible polymers: Progress and problems,” *J. Rheol.* **49**, 1–70 (2005).
- Liang, R. F. and M. R. Mackley, “Rheological characterization of the time and strain dependence for polyisobutylene solutions,” *J. Non-Newtonian Fluid Mech.* **52**, 387–405 (1994).
- McKinley, G. H. and T. Sridhar, “Filament-stretching rheometry of complex fluids,” *Ann. Rev. Fluid Mech.* **34**, 375–415 (2002).

- Phan-Thien, N., O. Manero and L. G. Leal, “A study of conformation-dependent friction in a dumbbell model for dilute solutions,” *Rheol. Acta* **23**, 151–162 (1984).
- Pincus, P., “Excluded volume effects and stretched polymer chains,” *Macromol.* **9**, 386–388 (1976).
- Prabhakar, R., *Predicting the rheological properties of dilute polymer solutions using bead-spring models: Brownian Dynamics simulations and closure approximations*, Monash University, Australia (2005).
- Prabhakar, R. and J. Prakash, “Multiplicative separation of the influences of excluded volume, hydrodynamic interactions and finite extensibility on the rheological properties of dilute polymer solutions,” *J. Non-Newtonian Fluid Mech.* **116**, 163–182 (2004).
- Prabhakar, R. and J. R. Prakash, “Gaussian approximation for finitely extensible bead-spring chains with hydrodynamic interaction,” *J. Rheol.* **50**, 561–593 (2006).
- Prabhakar, R., J. R. Prakash and T. Sridhar, “A successive fine-graining scheme for predicting the rheological properties of dilute polymer solutions,” *J. Rheol.* **48**, 1251–1278 (2004).
- Prabhakar, R., J. R. Prakash and T. Sridhar, “Effect of configuration-dependent intramolecular hydrodynamic interaction on elastocapillary thinning and breakup of filaments of dilute polymer solutions,” *J. Rheol.* **50**, 925–947 (2006).
- Radhakrishnan, R. and P. T. Underhill, “Models of flexible polymers in good solvents: relaxation and coil–stretch transition,” *Soft Matter* **8**, 2991–3003 (2012).
- Rubinstein, M. and R. H. Colby, *Polymer physics*, Oxford University Press, London, UK (2003).
- Schroeder, C. M., H. P. Babcock, E. S. G. Shaqfeh and S. Chu, “Observation of polymer conformation hysteresis in extensional flow,” *Science* **301**, 1515–1519 (2003).
- Schroeder, C. M., E. S. G. Shaqfeh and S. Chu, “Effect of hydrodynamic interactions on DNA dynamics in extensional flow: Simulation and single molecule experiment,” *Macromol.* **37**, 9242–9256 (2004).
- Somani, S., E. S. G. Shaqfeh and J. R. Prakash, “The effect of solvent quality on the coil-stretch transition,” *Macromol.* **43**, 10679–10691 (2010).
- Sridhar, T., D. A. Nguyen, R. Prabhakar and J. R. Prakash, “Rheological observation of glassy dynamics of dilute polymer solutions near the coil-stretch transition in elongational flows,” *Phys. Rev. Lett.* **98**, 167801 (2007).
- Stoltz, C., J. J. de Pablo and M. D. Graham, “Concentration dependence of shear and extensional rheology of polymer solutions: Brownian dynamics simulations,” *J. Rheol.* **50**, 137–167 (2006).

Tanner, R. I., “Stresses in dilute solutions of bead-nonlinear-spring macromolecules. III. Friction coefficient varying with dumbbell extension,” *J. Rheol.* **19**, 557–582 (1975).

Tirtaatmadja, V., G. H. McKinley and J. J. Cooper-White, “Drop formation and breakup of low viscosity elastic fluids: Effects of molecular weight and concentration,” *Phys. Fluids* **18**, 043101 (2006).